

Escherichia coli ribosomes support translation of (*R*) and (*S*) β^2 -hydroxyacids *in vitro*: a structural and biochemical study

Chandrima Majumdar¹, Alexandra D. Kent², Noah X. Hamlish¹, Cathy Zhu², Katelyn A. Fitzgerald¹, Alanna Schepartz^{1,2,3,4,5*}, Jamie H.D. Cate^{1,2,3,6*}

¹Department of Molecular and Cell Biology, University of California, Berkeley, CA 94720, USA;

²Department of Chemistry, University of California, Berkeley, CA 94720, USA;

³Molecular Biophysics and Integrated Bioimaging Division, Lawrence Berkeley National Laboratory, Berkeley, CA 94720, USA;

⁴Chan Zuckerberg Biohub, San Francisco, CA 94158, USA;

⁵Arc Institute, Palo Alto, CA

⁶Innovative Genomics Institute, University of California, Berkeley, CA 94720, USA.

*For correspondence: Tel: +15105417235; email: j-h-doudna-cate@berkeley.edu, schepartz@berkeley.edu

Abstract

The ribosomal incorporation of backbone-modified amino acid analogs into peptides and proteins enables the programmed synthesis of sequence-defined biopolymers with tunable properties. However, the successful use of backbone-modified monomers as substrates by the ribosome requires coordination across multiple parts of the translation machinery, including aminoacyl-tRNA synthetases, translation factors, and finally the ribosome itself. β -hydroxyacids are particularly interesting monomers because they have potential to support the programmed biosynthesis of both polyesters (plastics) and depsipeptides (therapeutics). Previous work has reported that both enantiomers of β^2 -hydroxy-N^ε-Boc-Lysine (β^2 -OH-BocK) are *in vitro* substrates for the orthogonal *M. alvi* PylRS/tRNA pair, but only one enantiomer is introduced into protein *in vivo* and with substantially lower yield than expected. We sought to determine whether there is a structural basis for the diminished yield as well as the preferential incorporation of one β^2 -OH-BocK enantiomer over the other. Here we report high-resolution cryo-EM structures of the *Escherichia coli* (*E. coli*) ribosome complexed with either (*R*)- or (*S*)- β^2 -OH-BocK. These structures reveal that both enantiomers are well positioned to undergo bond formation within the ribosome active site and are likely equally reactive. *In vitro* translation experiments confirm that orthogonal tRNAs acylated with (*R*)- or (*S*)- β^2 -OH-BocK are ribosome substrates, implying that the preferential incorporation of one enantiomer over the other *in vivo*

results from deficiencies in other translation steps, such as tRNA acylation efficiency in cells or delivery to the ribosome by elongation factor Tu (EF-Tu). Taken together, this work demonstrates the plasticity of the *E. coli* ribosome and its tolerance for diverse substrates.

Introduction

There is widespread interest in expanding the chemistry of the proteome using monomers that diverge from canonical or non-canonical α -amino acids.¹ Even seemingly minor substitutions in a peptide or protein, such as exchange of the α -amino group for an α -hydroxy group, can result in useful, emergent properties. Examples include discrete amide to ester substitutions that probe ion channel function or the role of backbone H-bonds in protein stability, and others that support intramolecular rearrangements to generate expanded or altered backbones.^{2–5} In a similar way, extension of the backbone with a non- α -amino acid such as a β^2 - or β^3 -amino acid can confer protease resistance, and improved thermodynamic stability in the context of both peptides and higher order assemblies.^{6–10} It is possible to introduce β^2 and β^3 backbones in ribosomal products post-translationally, either through a programmable O-N acyl shift rearrangement within the protein backbone or through tailoring enzymes.^{11,12} Yet introducing a β -amino acid into a protein directly *via* the ribosome is substantially more challenging than introducing an α -amino acid, whether canonical or otherwise, and especially in cells. The first example of a protein containing a β -amino acid produced in living cells (a β^3 -Phe derivative) was reported in 2016.¹³ Since that time, select β^2 -hydroxy acids and β^3 -amino acids have been introduced into proteins in cells, but the isolated yields of even model proteins containing a single β^2 - or β^3 -backbone are low, unpredictable, or both.^{14,15}

Previous work has shown that both the (*R*) and (*S*) stereoisomers of β^2 -OH-BocK are substrates for the *M. alvi* PylRS/tRNA^{Pyl} pair *in vitro*, but only one –(*R*)- β^2 -OH-BocK–is incorporated into proteins in cells and with a yield roughly 10-fold lower than expected based on aaRS activity.¹⁴ These differences could result from differences in tRNA acylation efficiency *in vivo*, how well the acyl-tRNAs are delivered to the ribosome, or how well the two stereoisomers are processed within the ribosome PTC.^{16,17} As there are currently no high-resolution structures of the ribosome in complex with any β^2 - or β^3 -hydroxy or amino acid, we sought to explore more deeply how β^2 -hydroxy acid monomers of opposite stereochemistry could be accommodated by the ribosome.

Here we describe two high resolution cryo-EM structures of the *E. coli* ribosome in complex with an A-site tRNA acylated with either (*R*) or (*S*)- β^2 -OH-BocK; in both structures the P site

contains tRNA acylated with L- α -fMet. Comparison of the two structures reveals that the pendant OH nucleophiles on tRNAs acylated with either (*R*) or (*S*)- β^2 -OH-BocK are positioned well for attack, with nucleophile-electrophile distances $< 3 \text{ \AA}$ and Burgi-Dunitz angles between 68° and 72° .¹⁸ Both side chains are inserted within the A-site cleft, and the PTC assumes the “induced” conformation seen in cryo-EM structures of ribosomes in complex with canonical A-site acyl-tRNAs. These observations suggest that both (*R*) and (*S*)- β^2 -OH-BocK have the potential for bond-forming reactions within the PTC, despite differences in stereochemistry. Indeed, when the two diastereomeric acyl-tRNAs are added in equal amounts to *in vitro* translation reactions, there is no statistical difference in how well each β^2 -OH-BocK monomer is incorporated into peptide. An observation consistent with previous reports that the WT *E. coli* ribosome can accept both stereoisomers of a β^2 -OH-acid *in vitro*.¹⁹ We propose that β^2 -backbones—regardless of stereochemistry—may be especially privileged substrates for the *E. coli* ribosome *in vivo* and that the incorporation of these monomers is limited by bottlenecks involving other parts of the translation machinery.

Results

Stereochemical resolution in cryo-EM structures of (*S*)- β^2 -OH-BocK and (*R*)- β^2 -OH-BocK within the ribosome

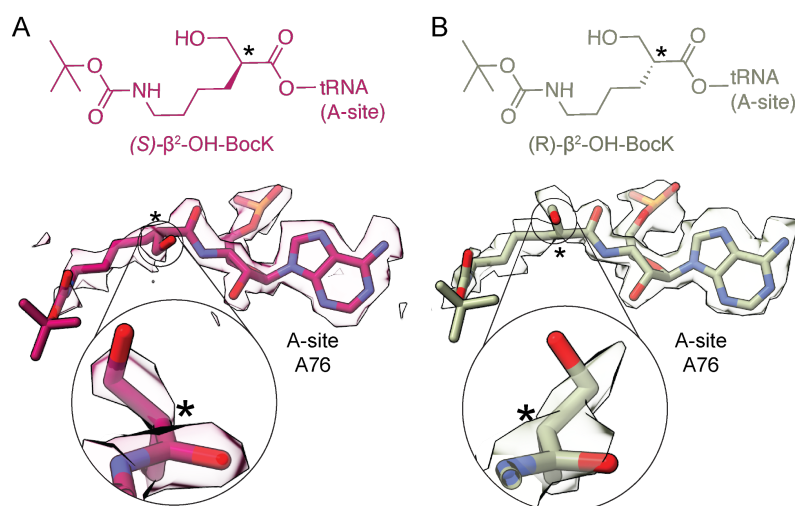


Figure 1: Chemical structures of **(A)** (*S*)- β^2 -OH-BocK and **(B)** (*R*)- β^2 -OH-BocK and cryo-EM densities of the corresponding acyl-tRNA termini when bound to the *E. coli* ribosome. Inset: Close-up view of stereocenter showing unambiguous density for each monomer. Each stereocenter is indicated by an asterisk.

To visualize how (*R*) and (*S*)- β^2 -OH-BocK are positioned within the ribosomal PTC, we obtained cryo-EM structures of the wild-type *E. coli* ribosome in complex with full-length acyl-tRNAs

occupying both the P and A sites. All acyl-tRNAs were prepared using tRNA molecules modified with a 3'-amino group (3'-NH₂-tRNA) to avoid acyl-tRNA hydrolysis during sample preparation (Supplementary Figure S1). Purified *E. coli* ribosomes were incubated with a 28-nucleotide mRNA, the P-site substrate fMet-NH-tRNA^{fMet} and one of two acylated A-site substrates ((*S*)-β²-OH-BocK-NH-tRNA^{Pyl} or (*R*)-β²-OH-BocK-NH-tRNA^{Pyl}). The structures of the two resulting complexes were solved using cryo-EM (Supplementary Figures S2 and S3). Initial rounds of 2D and 3D classification were performed to select intact 70S ribosomal particles (Supplementary Figures S4 and S5). The resulting cryo-EM maps contained complexes in the classical (non-rotated) state of the ribosome with clear density for both P- and A-site tRNAs. To improve the resolution of the (*R*) and (*S*)-β²-OH-BocK monomers, we further classified the ribosomal particles based on A-site tRNA occupancy. The final maps of 70S ribosomal particles containing A-site (*R*) or (*S*) β²-OH-BocK were refined to a global resolution of 2.14 Å and 2.29 Å, respectively (Supplementary Figures S2 and S3, Supplementary Tables S1 and S2). This resolution allowed for unambiguous modeling of A-site monomers in a single conformation and clear assignment of the stereochemistry of each enantiomer (Figure 1).²⁰

The ribosomal PTC adopts the “induced” conformation appropriate for bond formation when bound to tRNA acylated with either (*R*) or (*S*)-β²-OH-BocK

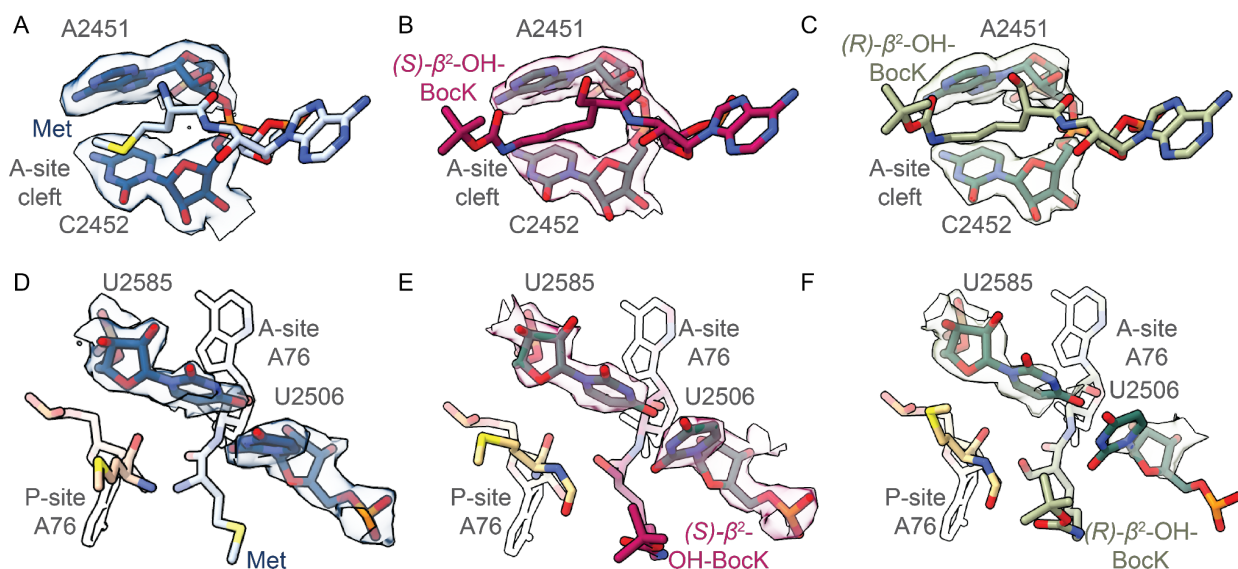


Figure 2: The ribosomal PTC adopts the “induced” conformation appropriate for bond formation when bound to tRNA acylated with either (*R*) or (*S*)-β²-OH-BocK. (A) Shown is a close-up view of Met-NH-tRNA^{fMet} bound within the PTC in the A site, with the Met side chain inserted into the A-site cleft formed

by nucleotides A2451 and C2452 (PDB: 8EMM). Analogous close-up views showing the placement of **(B)** (*S*)- and **(C)** (*R*)- β^2 -OH-BocK, whose side chains are similarly inserted into the A-site cleft. **(D)** Proper positioning of the A-site tRNA, as in the case of Met-NH-tRNA^{fMet}, results in the “induced” conformation of the ribosome that alters the placement of nucleotides U2585 and U2506 (PDB: 8EMM). As seen for canonical α -amino acids, accommodation of tRNAs acylated with either **(E)** (*S*)- or **(F)** (*R*)- β^2 -OH-BocK results in the proper “induced” conformation. In the ribosome complex carrying (*R*)- β^2 -OH-BocK, the density of the U2506 nucleobase is unresolved. Note: the displayed maps have a B-factor of 25 Å² applied for smoothness.

Upon delivery and proper accommodation within the ribosome, the A-site tRNA positions the incoming α -amino acid ester within the PTC through a base-pairing interaction between C75 of the A-site tRNA and G2553 within the A loop of the 23S rRNA.²¹ Previous structures of ribosomes containing tRNAs acylated with natural α -amino acids show the side chain of the amino acid accommodated within the A-site cleft, a wedge-shaped pocket created by the rRNA nucleotides A2451 and C2452 (Figure 2A).^{18,22–26} Cryo-EM structures of ribosomes in complex with tRNA acylated with either (*R*)- β^2 -OH-BocK or (*S*)- β^2 -OH-BocK show clear base pairing between G2553 in the A loop and C75 of the A-site tRNA. In addition, the BocK side chain of both monomers is inserted between residues A2451 and C2452, showing near-canonical positioning compared to natural L- α -amino acid side chains (Figure 2B,C). Due to the additional bulk of the Boc group, the side chain of these monomers is longer than natural amino acids and its density extends into the ribosome exit tunnel.

The proper accommodation of an acylated A-site tRNA within the PTC also results in conformational changes that facilitate bond formation between α -amino acid monomers that is commonly referred to as the “induced fit” mechanism. These conformational changes predominantly involve nucleotides U2506 and U2585.^{22,27} According to this mechanism, in the absence of a bound aminoacyl-tRNA, the ribosome exists in the uninduced state and U2506 forms a wobble base pair with G2583. Once an aminoacyl-tRNA is accommodated in the A site, the ribosome transitions to an induced state in which U2506 rotates to confine the side chain of the A-site α -amino acid within the A-site cleft and away from the reaction center (Figure 2D). The change in position of U2506 also places the nucleophilic α -amine of the A-site aminoacyl-tRNA within ~ 3 Å of the P-site ester carbonyl carbon and with a Burgi-Dunitz angle of $\sim 70^\circ$.

Previous structures of ribosomes in complex with non-natural acyl-tRNAs whose side chains cannot fully engage the A-site cleft (specifically, *o*, *m*, and *p*-aminobenzoic acids) do not show the structural rearrangements associated with the induced conformation.²⁶ Indeed, the absence of these structural rearrangements can be correlated with the decreased bond-forming efficiency in these three cases.²⁶ In contrast, tRNAs acylated with either (*R*)- β^2 -OH-BocK or (*S*)- β^2 -OH-BocK were accommodated in the PTC in a manner that fully supports the induced fit conformation of the ribosome (Figure 2E,F). One interesting detail is that the density for U2506 in the ribosome complex with tRNA acylated with (*S*)- β^2 -OH-BocK is weaker than with (*R*)- β^2 -OH-BocK, indicating that this nucleotide is more dynamic in the former complex.

The ribosomal P site contains an ordered water network when bound to tRNAs acylated with either (*R*) or (*S*)- β^2 -OH-BocK

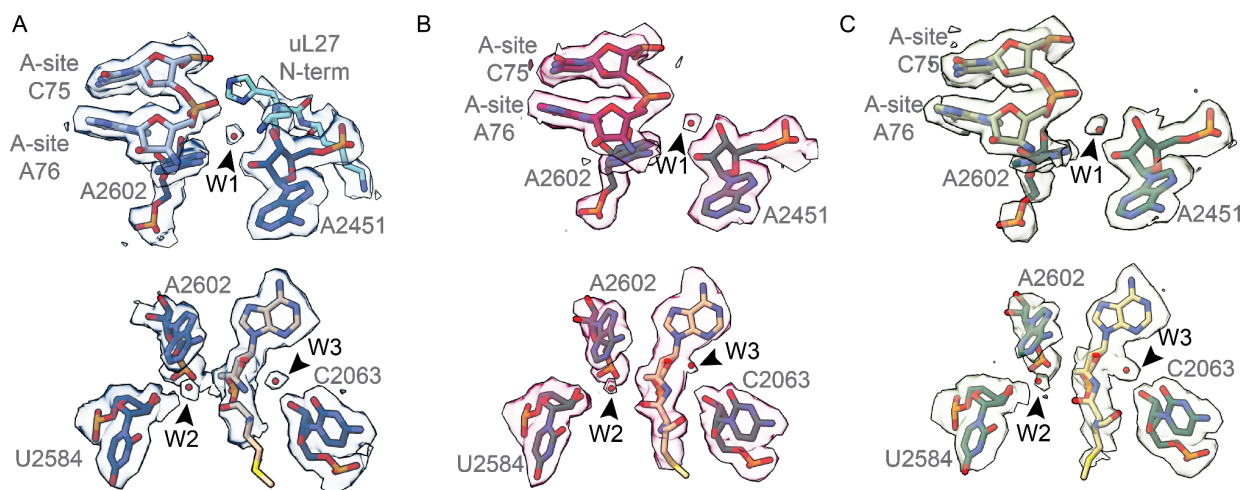


Figure 3: An ordered water network is established when the ribosome is bound to an A-site tRNA acylated with either (*R*) or (*S*)- β^2 -OH-BocK. (A) When the *E. coli* ribosome is bound to L- α -Met-NH-tRNA^{Met} in the P- and A-sites, three ordered water molecules, W1, W2 and W3 (indicated with black arrows) are in position to act as general acid and base catalysts and facilitate proton transfers between the reactants and ribosome (PDB:8EMM). (B), (C) W1, W2 and W3 are all present when the ribosome is bound to tRNA acylated with either (B) (*S*)- or (C) (*R*)- β^2 -OH-BocK, although we note that W3 has weaker cryo-EM density in (B) than in (C). Note: the displayed maps have a B-factor of 25 Å² applied for smoothness.

The nucleophilic attack of the A-site monomer on the P-site carbonyl group and the subsequent acyl-transfer reaction involves the shuttling of protons between the reactive groups and the

ribosome. These proton transfers are proposed to be mediated by a network of three ordered water molecules known as the “proton-wire” (Figure 3A).^{23,28} All three ordered water molecules of the proton wire have clear density in the complexes containing either (*R*)- or (*S*)- β^2 -OH-BocK (Figure 3B,C). The only difference in the proton wire that we detect is the density for W3, which has been proposed to transfer a proton to the 3'-oxygen of the P-site A76 ribose and facilitate the breakdown of the tetrahedral intermediate during amide bond formation. In the ribosome complex containing (*S*)- β^2 -OH-BocK, the density for W3 is weaker than in the (*R*)- β^2 -OH-BocK complex, suggesting that W3 is more dynamic in the former complex.

tRNAs acylated with either (*R*) or (*S*)- β^2 -OH-BocK position the nucleophilic OH group for bond formation

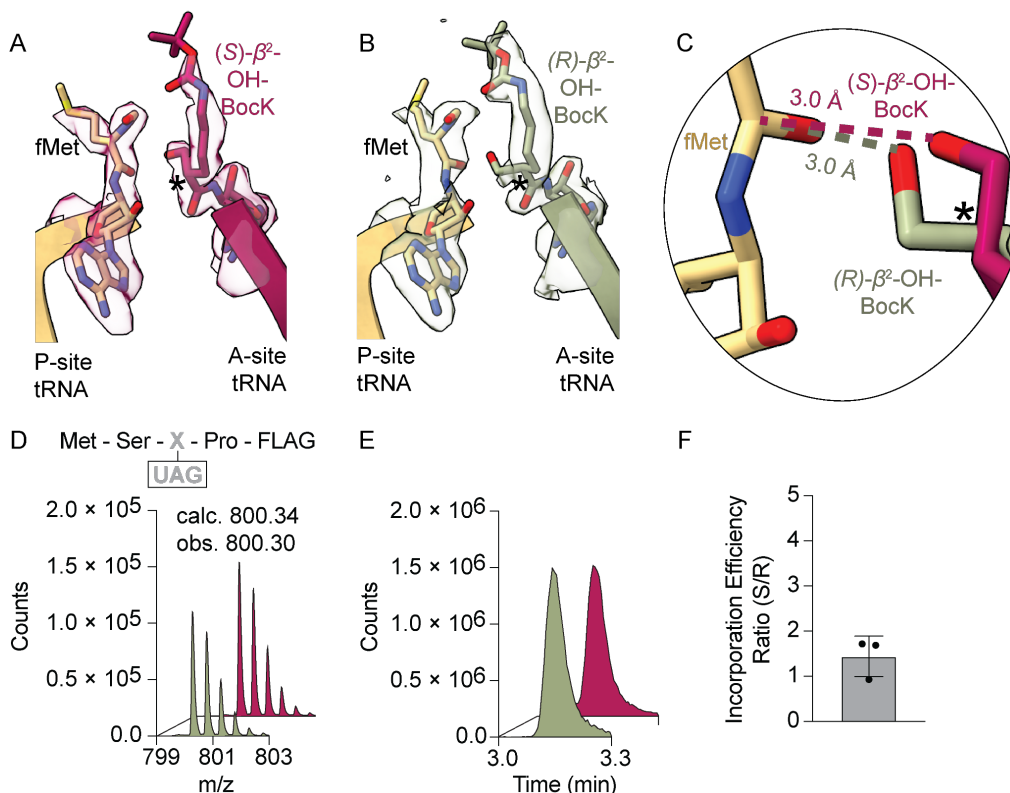


Figure 4: Relative position and reactivity of acyl-tRNAs containing (*R*) or (*S*)- β^2 -OH-BocK. The nucleophilic β^2 -OH oxygen atoms of acyl-tRNAs containing either (**A**) (*S*)- β^2 -OH-BocK or (**B**) (*R*)- β^2 -OH-BocK in the A site are positioned (**C**) 3.0 Å away from the electrophilic carbonyl group of the P-site fMet, suggesting that both substrates have the potential to react equally. Note: the displayed maps have a B-factor of 25 Å² applied for smoothness. (**D**) The relative reactivity of these two acyl-tRNAs was evaluated using *in vitro* translation (IVT) reactions programmed to generate the peptide Met-Ser-X-Pro-FLAG, where X is provided by tRNA^{Pyl} acylated with either (*S*)- β^2 -OH-BocK (maroon) or (*R*)- β^2 -OH-

BocK (green). Shown are the m/z spectra of the +2 ion detected in IVT reactions programmed with tRNA^{Pyl} acylated with (*S*)- β^2 -OH-BocK (maroon) or (*R*)- β^2 -OH-BocK (green) along with the calculated (calc.) and observed (obs.) masses and the (E) extracted ion chromatograms (EICs) of the corresponding FLAG-tag peptides. (F) The relative reactivity of the two acyl-tRNAs was taken as the ratio of the two EIC peaks shown in panel E. Error bars represent the standard deviation of three independent experiments.

The various interactions between PTC nucleotides and the acylated P- and A-site tRNAs ultimately position the A-site nucleophile and the P-site electrophile in close proximity within the PTC. When both contain a natural L- α -amino acid backbone, the nucleophilic α -amino group of the A-site monomer is positioned approximately 3 Å away from the electrophilic carbonyl carbon of the P-site peptidyl tRNA.^{18,23,27} When the A-site nucleophile contains a β^2 -backbone derived from either (*R*)- or (*S*)- β^2 -OH-BocK, because of the difference in absolute stereochemistry the carbon chains carrying the two OH nucleophiles point in opposite directions as they emerge from the chiral center (Figure 4A,B). However, the additional methylene group that defines the β^2 -linkage allows the two nucleophilic oxygen atoms to occupy the same position located 3 Å from the electrophilic carbonyl group of the P-site amino acid. Thus despite differences in absolute stereochemistry, when accommodated within the PTC both (*R*)- and (*S*)- β^2 -OH-BocK are positioned optimally for a bond formation (Figure 4C).

Monomer incorporation into peptides during *in vitro* translation.

Having established that the nucleophilic OH groups of both (*R*)- and (*S*)- β^2 -OH-BocK are positioned within the PTC in a manner appropriate for bond formation, we sought to determine how well these two monomers are introduced by the ribosome into peptide during *in vitro* translation reactions. Using purified *M. alvi* PylRS, we acylated tRNA^{Pyl} with BocK, (*S*)- β^2 -OH-BocK, or (*R*)- β^2 -OH-BocK, and quantified the percent of acylated tRNA using intact tRNA LC-MS (Supplementary Figure S5, S6 and Table S3).²⁹ We then used these values to charge IVT reactions with identical concentrations of monoacyl-tRNA, a DNA template encoding a stop codon (UAG) at the third position of a FLAG-tagged peptide product, and a PURE system lacking release factor 1 (Figure 4D and Table S5). Peptide products were detected and quantified using high-resolution LC-MS, with the counts from the extracted ion chromatogram normalized to those observed when an equivalent concentration of BocK-tRNA^{Pyl} was used to charge the IVT reaction (Figure 4E and Supplementary Figure S7). We found that (*S*)- β^2 -OH-BocK and (*R*)-

β^2 -OH-BocK were introduced into the FLAG-tagged peptide product with similar efficiencies, with a ratio of approximately 1:1 (Figure 4F) and an overall yield that is roughly ten-fold lower than that of an otherwise identical peptide containing BocK (Figure S8). The lack of significant difference in the relative incorporation of (*S*)- β^2 -OH-BocK and (*R*)- β^2 -OH-BocK during *in vitro* translation is fully consistent with the structural data described above, which shows the nucleophilic atoms of the two β^2 enantiomers positioned equidistant and in close proximity to the reactive P-site carbonyl (Figure 4C).

Discussion

Cryo-EM structures reveal that tRNAs acylated with either (*S*)- β^2 -OH-BocK or (*R*)- β^2 -OH-BocK are well accommodated within the PTC

This project was initiated to provide a better understanding of how enantiomeric β^2 -hydroxy acid monomers are accommodated within the PTC of wild type *E. coli* ribosomes. Although it has been shown that both the (*R*) and (*S*) enantiomers of β^2 -OH-BocK are substrates for the orthogonal *M. alvi* PylRS/tRNA^{Pyl} pair when assayed *in vitro*, only the (*R*)- β^2 -OH-BocK is introduced into a model protein in cells, and with a yield 10-fold lower than expected based on *in vitro* aaRS activity.²⁰ Metadynamics simulations performed using a reduced ribosome model failed to provide a clear-cut explanation for either difference in reactivity.^{14,18} Although ribosomes from many organisms have been characterized structurally at high resolution, there are currently no reported ribosome structures from any organism in complex with any β -backbone monomer. To fill this gap in knowledge, we made use of cryo-EM to determine the structure of the *E. coli* ribosome in complex with orthogonal tRNAs acylated with either (*R*)- or (*S*)- β^2 -OH-BocK. We were especially interested to visualize how tRNAs acylated with these enantiomeric monomers are accommodated within the PTC in comparison with native α -amino acids and whether there are fundamental or subtle differences in PTC interactions in the bound state.

The cryo-EM structures reported in this work show well-resolved density for both the A- and P-site tRNAs and their appended monomers and provide unambiguous stereochemical assignment

of the two β^2 -hydroxy-BocK isomers. Overall, despite the additional methylene group in their backbone, tRNAs acylated with β^2 -hydroxy-BocK monomers are accommodated within the PTC in a manner highly reminiscent of tRNAs acylated with natural L- α -amino acids. These native-like interactions include expected base pairing interactions between the A-site tRNA and the A loop and accommodation of the extended side chain within the A-site cleft (Figure 2).

tRNAs acylated with β^2 -hydroxy-BocK monomers also promote the canonical “induced fit” conformational changes within the PTC that position the nucleophile and electrophile to promote bond formation. In the absence of an A-site tRNA substrate, the ribosome exists in the uninduced state, and nucleotide U2585 is positioned close to the reactive P-site carbonyl protecting it from premature hydrolysis. In the presence of an appropriately bound A-site tRNA substrate, proper accommodation of the acylated tRNA breaks the wobble base pair between nucleobases U2506 and G2583 and nucleotides 2583-2585 are repositioned to reveal the P-site carbonyl and establish the “induced” state, ready for bond formation. tRNAs acylated with both (*R*) and (*S*) β^2 -OH-BocK elicit the induced state of the PTC and their reactive nucleophiles are positioned in close proximity to the P-site carbonyl. Ribosomes bound to tRNAs acylated with either (*R*)- and (*S*)- β^2 -OH-BocK also show all three water molecules associated with the “proton-wire” that is believed to support general acid/base during each catalytic cycle.

Although tRNAs acylated with either (*R*)- or (*S*)- β^2 -OH-BocK elicit an induced PTC state, tRNAs acylated with other non- α -amino acid monomers do not.²⁶ Previous structures of ribosomes whose tRNAs are acylated with *o*, *m*, or *p*-aminobenzoic acid are distinguished by a steric clash between the conformationally constrained aromatic backbone and nucleotide U2506. As a result, the ribosome remains in the uninduced state, providing a clear explanation for the relatively poor efficiency of bond formation by these monomers.

Positioning of β^2 -OH-BocK nucleophiles relative to P-site carbonyl

In these and previous structures, we observed that two geometrical restraints anchor the A-site monomer within the PTC and dictate its overall position. The first is the acyl linkage between the monomer and the 3'-oxygen/nitrogen of A76 of the A-site tRNA. The second is the

accommodation of the A-site monomer side chain within the A-site cleft. Together, these constraints limit the positional space of the A-site nucleophile. When the A-site tRNA is acylated with an L- or D- α -amino acid, the difference in stereochemistry orients only the nucleophile of the L- α -amino acid to attack the P-site carbonyl, providing a clear structural rationale for the diminished reactivity of D- α -amino acid monomers during translation.²⁴ However, when the A-site tRNA is acylated with a β^2 -hydroxy acid, there is an additional methylene group ($-\text{CH}_2-$) separating the stereogenic carbon and the nucleophile. This additional atom and the degrees of freedom associated with it allow both β^2 -hydroxy acid enantiomers to adopt a conformation in which the nucleophilic oxygen is positioned within 3 Å, i.e. bond forming distance, of the electrophilic carbonyl group (Figure 4C). As a result, based on the structures alone, both enantiomers are predicted to be equally reactive once delivered to and accommodated within the ribosome PTC.

***In vitro* results confirm that (*R*)- β^2 -OH-BocK and (*S*)- β^2 -OH-BocK are equally reactive**

To test this prediction, we used *in vitro* translation reactions to assess the relative reactivity of tRNAs acylated with either (*R*)- β^2 -OH-BocK and (*S*)- β^2 -OH-BocK. Using internally controlled reactions and equivalent concentrations of each acyl-tRNA, we found that *in vitro* there is no significant difference in incorporation efficiency (Figure 4D-F), in full support of the cryo-EM structures reported herein. Notably, as observed in cells, (*R*) and (*S*)- β^2 -OH-BocK were both incorporated into peptide via IVT with roughly 10-fold lower efficiency than BocK (Figure S7).¹⁴

What then accounts for the differences in incorporation observed in cells and *in vitro*? We hypothesize that EF-Tu is at least partially responsible, as this essential translation factor forms weaker ternary complexes with β^2 -Phe-tRNA^{Phe} than with L- α -Phe-tRNA^{Phe} (weaker ternary complexes are also observed for the analogous β^3 -Phe derivatives).¹⁷ The apparent higher reactivity of (*R*)- β^2 -OH-BocK in cells appears to result from differences in tRNA acylation levels as quantified using mass spectrometry and a new assay called PARTI.¹⁶

The structures reported here also highlight that the A-site cleft, by accommodating the side chain of the monomer, or α -amino acid, plays a significant role in dictating the overall positioning of the monomer and orienting the reactive nucleophile. Indeed, monomers carrying nucleophiles closer to the side chain, such as β^3 -amino acids, are likely to have these nucleophiles positioned much farther away from the P-site carbonyl group than in the case of α -amino acids, thereby leading to reduced reactivity.

Overall, the structures reported here demonstrate the plasticity of the *E. coli* ribosome and its tolerance for diverse substrates. We anticipate that these structures will help guide the design of novel monomers that are well accommodated within the PTC and positioned optimally to support bond formation within the ribosome.

Associated Content

Supporting Information

The Supporting Information is available free of charge at https://pubs.acs.org/doi/_____

Materials and methods, cryo-EM data collection and model refinement statistics, mass spectrometry traces of tRNA acylation and peptide quantification, supplementary figures.

Accession Codes

Atomic coordinates have been deposited with the Protein Data Bank under accession codes 9O2X and 9O2Y (for *(S)*- β^2 -OH-BocK and *(R)*- β^2 -OH-BocK respectively). Cryo-EM maps have been deposited with the Electron Microscopy Data Bank under the accession codes EMD-70051 (composite 70S map for *(S)*- β^2 -OH-BocK), EMD-70052 (50S focus refined map for *(S)*- β^2 -OH-BocK), EMD - 70054 (30S focus refined map for *(S)*- β^2 -OH-BocK), EMD-70477(global map 70S for *(S)*- β^2 -OH-BocK), EMD-70051 (composite 70S map for *(R)*- β^2 -OH-BocK), EMD-70055 (50S focus refined map for *(R)*- β^2 -OH-BocK), EMD - 70056 (30S focus refined map for *(R)*- β^2 -OH-BocK), and EMD-70478 (global 70S map for *(R)*- β^2 -OH-BocK).

Acknowledgements

This work was supported by the NSF Center for Genetically Encoded Materials, CHE-2002182. We also thank Dr. Dan Toso, Dr. Ravindra Thakkar, and Paul Tobias for help with cryo-EM data collection and management.

References

- (1) Kwon, D. How Scientists Are Hacking the Genetic Code to Give Proteins New Powers. *Nature* **2023**, *618* (7966), 874–876. <https://doi.org/10.1038/d41586-023-01980-4>.
- (2) Schissel, C. K.; Roberts-Mataric, H.; Garcia, I. J.; Kang, H.; Mowzoon-Mogharrabi, R.; Francis, M. B.; Schepartz, A. Peptide Backbone Editing via Post-Translational O to C Acyl Shift. *J. Am. Chem. Soc.* **2025**. <https://doi.org/10.1021/jacs.4c14103>.
- (3) Knudson, I. J.; Dover, T. L.; Dilworth, D. A.; Paloutzian, C.; Cho, H.; Schepartz, A.; Miller, S. J. Chemo-Ribosomal Synthesis of Atropisomeric and Macrocyclic Peptides with Embedded Quinolines. ChemRxiv June 10, 2024. <https://doi.org/10.26434/chemrxiv-2024-kvdpq>.
- (4) England, P. M.; Zhang, Y.; Dougherty, D. A.; Lester, H. A. Backbone Mutations in Transmembrane Domains of a Ligand-Gated Ion Channel: Implications for the Mechanism of Gating. *Cell* **1999**, *96* (1), 89–98.
- (5) Guo, J.; Wang, J.; Anderson, J. C.; Schultz, P. G. Addition of an α -Hydroxy Acid to the Genetic Code of Bacteria. *Angew. Chem. Int. Ed.* **2008**, *47* (4), 722–725. <https://doi.org/10.1002/anie.200704074>.
- (6) Cabrele, C.; Martinek, T. A.; Reiser, O.; Berlicki, Ł. Peptides Containing β -Amino Acid Patterns: Challenges and Successes in Medicinal Chemistry. *J. Med. Chem.* **2014**, *57* (23), 9718–9739. <https://doi.org/10.1021/jm5010896>.
- (7) Seebach, D.; Gardiner, J. β -Peptidic Peptidomimetics. *Acc. Chem. Res.* **2008**, *41* (10), 1366–1375. <https://doi.org/10.1021/ar700263g>.
- (8) Cheloha, R. W.; Maeda, A.; Dean, T.; Gardella, T. J.; Gellman, S. H. Backbone Modification of a Polypeptide Drug Alters Duration of Action in Vivo. *Nat. Biotechnol.* **2014**, *32* (7), 653–655. <https://doi.org/10.1038/nbt.2920>.
- (9) Hager, M. V.; Clydesdale, L.; Gellman, S. H.; Sexton, P. M.; Wootten, D. Characterization of Signal Bias at the GLP-1 Receptor Induced by Backbone Modification of GLP-1. *Biochem. Pharmacol.* **2017**, *136*, 99–108. <https://doi.org/10.1016/j.bcp.2017.03.018>.
- (10) Hager, M. V.; Johnson, L. M.; Wootten, D.; Sexton, P. M.; Gellman, S. H. β -Arrestin-Biased Agonists of the GLP-1 Receptor from β -Amino Acid Residue Incorporation into GLP-1 Analogues. *J. Am. Chem. Soc.* **2016**, *138* (45), 14970–14979. <https://doi.org/10.1021/jacs.6b08323>.
- (11) Roe, L. T.; Schissel, C. K.; Dover, T. L.; Shah, B.; Hamlish, N. X.; Zheng, S.; Dilworth, D. A.; Wong, N.; Zhang, Z.; Chatterjee, A.; Francis, M. B.; Miller, S. J.; Schepartz, A. Backbone Extension Acyl Rearrangements Enable Cellular Synthesis of Proteins with Internal B₂-Peptide Linkages. bioRxiv October 4, 2023, p 2023.10.03.560714. <https://doi.org/10.1101/2023.10.03.560714>.
- (12) Morinaka, B. I.; Lakis, E.; Verest, M.; Helf, M. J.; Scalvenzi, T.; Vagstad, A. L.; Sims, J.; Sunagawa, S.; Gugger, M.; Piel, J. Natural Noncanonical Protein Splicing Yields Products with Diverse β -Amino Acid Residues. *Science* **2018**, *359* (6377), 779–782. <https://doi.org/10.1126/science.aao0157>.
- (13) Melo Czekster, C.; Robertson, W. E.; Walker, A. S.; Söll, D.; Schepartz, A. In Vivo Biosynthesis of a β -Amino Acid-Containing Protein. *J. Am. Chem. Soc.* **2016**, *138* (16), 5194–5197. <https://doi.org/10.1021/jacs.6b01023>.
- (14) Hamlish, N. X.; Abramyan, A. M.; Shah, B.; Zhang, Z.; Schepartz, A. Incorporation of Multiple B₂-Hydroxy Acids into a Protein In Vivo Using an Orthogonal Aminoacyl-tRNA Synthetase. *ACS Cent. Sci.* **2024**, *10* (5), 1044–1053. <https://doi.org/10.1021/acscentsci.3c01366>.
- (15) Dunkelmann, D. L.; Piedrafita, C.; Dickson, A.; Liu, K. C.; Elliott, T. S.; Fiedler, M.; Bellini, D.; Zhou, A.; Cervettini, D.; Chin, J. W. Adding α,α -Disubstituted and β -Linked Monomers

- to the Genetic Code of an Organism. *Nature* **2024**, 625 (7995), 603–610. <https://doi.org/10.1038/s41586-023-06897-6>.
- (16) Pressimone, M. A.; Schissel, C. K.; Goss, I. H.; Swenson, C. V.; Schepartz, A. Monitoring Monomer-Specific Acyl-tRNA Levels in Cells with PARTI. *bioRxiv* **2025**, 2025.01.14.633079. <https://doi.org/10.1101/2025.01.14.633079>.
- (17) Cruz-Navarrete, F. A.; Griffin, W. C.; Chan, Y.-C.; Martin, M. I.; Alejo, J. L.; Brady, R. A.; Natchiar, S. K.; Knudson, I. J.; Altman, R. B.; Schepartz, A.; Miller, S. J.; Blanchard, S. C. β -Amino Acids Reduce Ternary Complex Stability and Alter the Translation Elongation Mechanism. *ACS Cent. Sci.* **2024**, 10 (6), 1262–1275. <https://doi.org/10.1021/acscentsci.4c00314>.
- (18) Watson, Z. L.; Knudson, I. J.; Ward, F. R.; Miller, S. J.; Cate, J. H. D.; Schepartz, A.; Abramyan, A. M. Atomistic Simulations of the Escherichia Coli Ribosome Provide Selection Criteria for Translationally Active Substrates. *Nat. Chem.* **2023**, 15 (7), 913–921. <https://doi.org/10.1038/s41557-023-01226-w>.
- (19) Sando, S.; Abe, K.; Sato, N.; Shibata, T.; Mizusawa, K.; Aoyama, Y. Unexpected Preference of the E. Coli Translation System for the Ester Bond during Incorporation of Backbone-Elongated Substrates. *J. Am. Chem. Soc.* **2007**, 129 (19), 6180–6186. <https://doi.org/10.1021/ja068033n>.
- (20) The samples of (*R*)- and (*S*)- β^2 -OH-Bock used in this work were obtained from Enamine, but the absolute stereochemistries of the two isomers were mis-assigned. The correct assignments were established by the cryo-EM structures reported herein. A correction of the original report of Hamlish *et al.* has been submitted and is provided as Supplementary Material.
- (21) Kim, D. F.; Green, R. Base-Pairing between 23S rRNA and tRNA in the Ribosomal A Site. *Mol. Cell* **1999**, 4 (5), 859–864. [https://doi.org/10.1016/S1097-2765\(00\)80395-0](https://doi.org/10.1016/S1097-2765(00)80395-0).
- (22) Martin Schmeing, T.; Huang, K. S.; Strobel, S. A.; Steitz, T. A. An Induced-Fit Mechanism to Promote Peptide Bond Formation and Exclude Hydrolysis of Peptidyl-tRNA. *Nature* **2005**, 438 (7067), 520–524. <https://doi.org/10.1038/nature04152>.
- (23) Polikanov, Y. S.; Steitz, T. A.; Innis, C. A. A Proton Wire to Couple Aminoacyl-tRNA Accommodation and Peptide-Bond Formation on the Ribosome. *Nat. Struct. Mol. Biol.* **2014**, 21 (9), 787–793. <https://doi.org/10.1038/nsmb.2871>.
- (24) Melnikov, S. V.; Khabibullina, N. F.; Mairhofer, E.; Vargas-Rodriguez, O.; Reynolds, N. M.; Micura, R.; Söll, D.; Polikanov, Y. S. Mechanistic Insights into the Slow Peptide Bond Formation with D-Amino Acids in the Ribosomal Active Site. *Nucleic Acids Res.* **2019**, 47 (4), 2089–2100. <https://doi.org/10.1093/nar/gky1211>.
- (25) Melnikov, S.; Mailliot, J.; Rigger, L.; Neuner, S.; Shin, B.-S.; Yusupova, G.; Dever, T. E.; Micura, R.; Yusupov, M. Molecular Insights into Protein Synthesis with Proline Residues. *EMBO Rep.* **2016**, 17 (12), 1776–1784. <https://doi.org/10.15252/embr.201642943>.
- (26) Majumdar, C.; Walker, J. A.; Francis, M. B.; Schepartz, A.; Cate, J. H. D. Aminobenzoic Acid Derivatives Obstruct Induced Fit in the Catalytic Center of the Ribosome. *ACS Cent. Sci.* **2023**, 9 (6), 1160–1169. <https://doi.org/10.1021/acscentsci.3c00153>.
- (27) Lehmann, J. Induced Fit of the Peptidyl-Transferase Center of the Ribosome and Conformational Freedom of the Esterified Amino Acids. *RNA* **2017**, 23 (2), 229–239. <https://doi.org/10.1261/rna.057273.116>.
- (28) Kazemi, M.; Sočan, J.; Himo, F.; Åqvist, J. Mechanistic Alternatives for Peptide Bond Formation on the Ribosome. *Nucleic Acids Res.* **2018**, 46 (11), 5345–5354. <https://doi.org/10.1093/nar/gky367>.
- (29) Fricke, R.; Knudson, I.; Schepartz, A. Direct, Quantitative, and Comprehensive Analysis of tRNA Acylation Using Intact tRNA Liquid-Chromatography Mass-Spectrometry. *bioRxiv* July 14, 2023, p 2023.07.14.549096. <https://doi.org/10.1101/2023.07.14.549096>.

Supplementary Information

Escherichia coli ribosomes support translation of (*R*) and (*S*) β^2 -hydroxyacids *in vitro*: a structural and biochemical study

Chandrima Majumdar¹, Alexandra D. Kent², Noah X. Hamlish¹, Cathy Zhu², Katelyn A. Fitzgerald¹, Alanna Schepartz^{1,2,3,4,5*}, Jamie H.D. Cate^{1,2,3,6*}

¹Department of Molecular and Cell Biology, University of California, Berkeley, CA 94720, USA;

²Department of Chemistry, University of California, Berkeley, CA 94720, USA;

³Molecular Biophysics and Integrated Bioimaging Division, Lawrence Berkeley National Laboratory, Berkeley, CA 94720, USA;

⁴Chan Zuckerberg Biohub, San Francisco, CA 94158, USA;

⁵Arc Institute, Palo Alto, CA

⁶Innovative Genomics Institute, University of California, Berkeley, CA 94720, USA.

*For correspondence: Tel: +15105417235; email: j-h-doudna-cate@berkeley.edu, schepartz@berkeley.edu

1. Materials and Methods

- a. Source and stereochemical assignment of (*R*) and (*S*)- β^2 -OH-BocK
- b. Transcription of tRNA^{fMet}(-A) and tRNA^{Pyl}(-A)
- c. Preparation of tRNA molecules carrying a 3'-amino group: 3'-NH₂-tRNA^{fMet} and 3'-NH₂-tRNA^{Pyl}
- d. Enzymatic acylation of 3'-NH₂-tRNA^{fMet} with fMet
- e. Enzymatic acylation of tRNA^{Pyl} and with BocK and (*R*)- β^2 -OH-BocK
- f. Enzymatic acylation of tRNA^{Pyl} and with BocK and (*S*)- β^2 -OH-BocK
- g. Enzymatic acylation of 3'-OH-tRNA^{Pyl} with BocK, (*S*)- β^2 -OH-BocK, or (*R*)- β^2 -OH-BocK
- h. Characterization of Acylated 3'-NH₂-tRNA^{fMet}, 3'-NH₂-tRNA^{Pyl} and tRNA^{Pyl}
- i. Cryo-EM complex preparation
- j. Cryo-EM sample preparation
- k. Cryo-EM data collection
- l. Image Processing
- m. Pixel Size Calibration
- n. Modeling

- o. *In vitro* translation of peptides containing (*R*) and (*S*)- β^2 -OH-BocK
 - p. Purification and analysis of FLAG-tagged peptides containing (*R*) and (*S*)- β^2 -OH-BocK
2. Supplementary figures
- a. Figure S1: Intact tRNA LC-MS of 3'-NH₂-tRNA^{Pyl} acylated with β^2 -OH-BocK
 - b. Figure S2: Cryo-EM data processing workflow for complex whose A-site tRNA is acylated by (*S*)- β^2 -OH-BocK.
 - c. Figure S3: Cryo-EM data processing workflow for complex whose A-site tRNA is acylated by (*R*)- β^2 -OH-BocK.
 - d. Figure S4: Resolution of the 70S of the complex whose A-site tRNA is acylated by (*R*)- β^2 -OH-BocK.
 - e. Figure S5: Resolution of the 70S of the complex whose A-site tRNA is acylated by (*S*)- β^2 -OH-BocK.
 - f. Figure S6: Intact tRNA LC-MS of tRNA^{Pyl} acylated with BocK, (*R*)- β^2 -OH-BocK, or (*S*)- β^2 -OH-BocK, replicate 1.
 - g. Figure S7: Intact tRNA LC-MS of tRNA^{Pyl} acylated with BocK, (*R*)- β^2 -OH-BocK, or (*S*)- β^2 -OH-BocK, replicate 2.
 - h. Figure S8: Incorporation of BocK, (*S*)- β^2 -OH-BocK, or (*R*)- β^2 -OH-BocK into a peptide using *in vitro* transcription/translation.
3. Supplementary tables
- a. Table S1: Data collection and processing of WT *E. coli* ribosome complexes with β^2 -OH-BocK monomers.
 - b. Table S2: Model Refinement Statistics for WT *E. coli* ribosome complexes with β^2 -OH-BocK monomers.
 - c. Table S3: Quantification of acylation from Supplementary Figures S6-S7 and corresponding IVTT replicates.
 - d. Table S5: Sequences of RNA oligomers used in this study
 - e. Table S6: Sequences of DNA primers used in this study.
 - f. Table S7: Sequences of peptides used in this study.

4. References

1. Materials and Methods

a. Source and assignment of (*R*)- and (*S*)- β^2 -OH-BocK

(*R*)- and (*S*)- β^2 -OH-BocK were obtained from Enamine, but the absolute stereochemistry was misassigned by the supplier. The correct assignments were established upon cryo-EM analysis of the structures reported herein. A correction to the initial report in *ACS Cent Sci* has been submitted.

b. Transcription of $tRNA^{fMet}(-A)$, $tRNA^{Pyl}$ and $tRNA^{Pyl}(-A)$

Using previously described protocols, DNA templates for *E. coli* $tRNA^{fMet}(-A)$ with a C1G mutation (to improve transcription yield) and *M. alvi* $tRNA^{Pyl}(-A)$ (Table S4) were prepared using a double PCR amplification method described previously.^{1,2} Briefly, long overlapping primers, fMet_C1G_temp_Fw and fMet_C1G_temp_Rv(-A) for $tRNA^{fMet}(-A)$, or Pyl_temp_Fw and Pyl_temp_Rv for $tRNA^{Pyl}(-A)$ (Table S4) were PCR amplified using Q5 polymerase (NEB). The PCR products were agarose gel purified and amplified using short primers fMet_C1G_amp_Fw and fMet_C1G_amp_Rv(-A) for $tRNA^{fMet}$ and Pyl_amp_Fw and Pyl_amp_Rv(-A) for $tRNA^{Pyl}$ using Q5 DNA polymerase (NEB). Amplification reactions were cleaned up using the DNA clean and concentrator-5 kit (Zymo research). The amplified PCR products were quantified by measuring the absorbance at 260 nm using a Nanodrop One (ThermoScientific). $tRNA^{fMet}(-A)$ and $tRNA^{Pyl}(-A)$ were *in vitro* transcribed in transcription buffer (50 mM Tris-HCl pH 7.5, 15 mM MgCl₂, 5 mM DTT, 2 mM spermidine), 10 mM NTPs (Promega), 1 U/ μ L murine RNase inhibitor (NEB), 0.5 U/ μ L T7 RNA polymerase ver.2.0 (Takara), 0.5 U/ μ L YIPP (NEB), and 3-5 μ g of DNA template per 200 μ L. Reactions were incubated at 37 °C for 2 hours. The tRNAs were then precipitated using EtOH and purified using a 12% polyacrylamide, 7 M urea, 1X TBE (100 mM Tris, 100 mM boric acid, 2 mM EDTA disodium salt) gel. Gel slices were excised and tRNAs extracted by crushing and soaking the gel in 300 mM NaOAc pH 5.2 overnight. The tRNAs were then precipitated in EtOH, the pellets dried, and then resuspended in nuclease-free water prior to storage at -80 °C.

c. Preparation of tRNA molecules carrying a 3'-amino group, 3'-NH₂- $tRNA^{fMet}$ and 3'-NH₂- $tRNA^{Pyl}$

$tRNA^{fMet}(-A)$ and $tRNA^{Pyl}(-A)$ were converted into 3'-NH₂- $tRNA^{fMet}$ and 3'-NH₂- $tRNA^{Pyl}$ using 2'-amino-2'-deoxyadenosine-5'-triphosphate (Axxora) and *E. coli* CCA adding enzyme using

previously described protocols.¹ Successful elongation to generate 3'-NH₂-tRNA^{fMet} and 3'-NH₂-tRNA^{Pyl} was confirmed by mass spectrometry.

d. Enzymatic acylation of 3'-NH₂-tRNA^{fMet} with fMet

3'-NH₂-tRNA^{fMet} was enzymatically aminoacylated using methionyl-tRNA synthetase (MetRS)^{3,4} and methionyl-tRNA formyltransferase (MTF) (gifts from Fred Ward, Cate lab). 10 μM 3'-NH₂-tRNA^{fMet} was incubated with 1 μM MetRS and 1 μM MTF in aminoacylation buffer (50 mM HEPES pH 7.5, 20 mM MgCl₂, 10 mM KCl, 2 mM dithiothreitol (DTT), 10 mM ATP) along with 1:40 volume murine RNase inhibitor (NEB), 10 mM methionine, and 300 μM 10-formyltetrahydrofolate.⁵ The reactions were incubated at 37 °C for 30 minutes, extracted with phenol chloroform, and precipitated with ethanol. Charging was confirmed by intact tRNA mass spectrometry. The charged fMet-NH-tRNA^{fMet} was stored in nuclease free water at -80 °C prior to use.

e. Enzymatic acylation of 3'-NH₂-tRNA^{Pyl} with (R)-β²-OH-BocK

3'-NH₂-tRNA^{Pyl} was enzymatically acylated with (R)-β²-OH-BocK using pyrrolysine-tRNA synthetase (PylRS). 10 μM 3'-NH₂-tRNA^{Pyl} was incubated with 12.5 μM PylRS in aminoacylation buffer (100 mM HEPES pH 7.5, 10 mM MgCl₂, 4 mM DTT, and 10 mM ATP) along with 0.004 U/μL inorganic pyrophosphatase (NEB) and 5 mM of (R)-β²-OH-BocK. Acylation reactions were incubated at 37 °C for 5 hrs after which additional fresh PylRS was added to the reaction to a concentration of 2.5 μM. Reactions were left to proceed overnight (16 hrs) at 37 °C and subsequently purified using a Zymo RNA Clean and Concentrate kit. Acylation was confirmed and quantified by intact tRNA mass spectrometry, indicating that the 3'-NH₂-tRNA^{Pyl} had been acylated with (R)-β²-OH-BocK with 98% yield. (Supplementary Figure S1).

f. Enzymatic acylation of 3'-NH₂-tRNA^{Pyl} with (S)-β²-OH-BocK

3'-NH₂-tRNA^{Pyl} was enzymatically acylated with (S)-β²-OH-BocK using pyrrolysine-tRNA synthetase (PylRS) in a similar manner to (R)-β²-OH-BocK albeit with considerably more forcing conditions to achieve sufficient acyl-tRNA for cryo-EM. 10 μM 3'-NH₂-tRNA^{Pyl} was incubated with 12.5 μM PylRS in aminoacylation buffer (100 mM HEPES pH 7.5, 10 mM MgCl₂, 4 mM DTT, and 10 mM ATP) along with 0.004 U/μL inorganic pyrophosphatase (NEB) and 5 mM of (R)-β²-OH-BocK. Acylation reactions were incubated at 37 °C for 5 hrs after which

additional fresh PylRS was added to the reaction to a concentration of 2.5 μM . Reactions were left to proceed overnight (19 hrs) at 37 $^{\circ}\text{C}$. 24 hrs after the acylation reaction was initiated, total tRNA was purified using a Zymo RNA Clean and Concentrate kit. Acylation was confirmed and quantified by intact tRNA mass spectrometry, indicating that the 3'-NH₂-tRNA^{Pyl} had been acylated with (*S*)- β^2 -OH-BocK with 69% yield. Total tRNA was then added to a fresh acylation reaction using the same reagent concentrations as above and incubated at 37 $^{\circ}\text{C}$ for 24 h. Total tRNA was subsequently purified using a Zymo RNA Clean and Concentrate kit and acyl-tRNA yield was calculated to be 81% by intact tRNA mass spectrometry. Total tRNA was then “re-fed” into a fresh acylation reaction two more times, each lasting 24 hrs. Acyl-tRNA yield after 4 total rounds of acylation afforded 3'-NH₂-tRNA^{Pyl} acylated with (*S*)- β^2 -OH-BocK in 94% yield. Acylation was confirmed and quantified by intact tRNA mass spectrometry (Supplementary Figure S1).

*g. Enzymatic acylation of 3'-OH-tRNA^{Pyl} with BocK, (*S*)- β^2 -OH-BocK, or (*R*)- β^2 -OH-BocK*
3'-OH-tRNA^{Pyl} was enzymatically acylated with BocK, (*S*)- β^2 -OH-BocK, or (*R*)- β^2 -OH-BocK using PylRS. 3'-OH-tRNA^{Pyl} was incubated with 12.5 μM PylRS in aminoacylation buffer (100 mM HEPES pH 7.5, 10 mM MgCl₂, 4 mM DTT, and 10 mM ATP) along with 0.004 U/ μL inorganic pyrophosphatase and 5 mM of BocK, (*S*)- β^2 -OH-BocK, or (*R*)- β^2 -OH-BocK. The reactions were incubated at 37 $^{\circ}\text{C}$ for 2 hrs and purified using a Zymo RNA Clean and Concentrate kit. To reduce the amount of tRNA^{Pyl} diacylated with (*R*)- β^2 -OH-BocK, we repeated acylations with the same conditions as above except for using 5 μM PylRS and incubating for only 1 hr. This afforded a 2.5-fold decrease in diacyl-tRNA^{Pyl} (from ~50% to ~20% of the total tRNA pool) with no effect on the monoacyl-tRNA^{Pyl} yield. Acylation was confirmed and quantified by intact tRNA mass spectrometry (Supplementary Figure S1).

h. Characterization of Acylated 3'-NH₂-tRNA^{Met}, 3'-NH₂-tRNA^{Pyl} and tRNA^{Pyl}
The identity of acylated 3'-NH₂-tRNA^{Met}, 3'-NH₂-tRNA^{Pyl} and tRNA^{Pyl} were confirmed as previously described.⁶ Samples were resolved on a ACQUITY UPLC BEH C18 Column (130 \AA , 1.7 μm , 2.1 mm X 50 mm, Waters part # 186002350, 60 $^{\circ}\text{C}$) using an ACQUITY UPLC I-Class PLUS (Waters part # 186015082). The mobile phases used were 8 mM triethylamine (TEA), 80 mM hexafluoroisopropanol (HFIP), 5 μM ethylenediaminetetraacetic acid (EDTA, free acid) in

MilliQ water (solvent A); and 4 mM TEA, 40 mM HFIP, 5 μ M EDTA (free acid) in 50% MilliQ water/50% methanol (solvent B). The method used a flow rate of 0.3 mL/min and began with Mobile Phase B at 22% that increased linearly to 40 % B over 10 min, followed by a linear gradient from 40 to 60% B for 1 min, a hold at 60% B for 1 min, a linear gradient from 60 to 22% B over 0.1 min, then a hold at 22% B for 2.9 min. The mass of the RNA was analyzed using LC-HRMS with a Waters Xevo G2-XS ToF (Waters part #186010532) in negative ion mode with the following parameters: capillary voltage: 2000 V, sampling cone: 40, source offset: 40, source temperature: 140 °C, desolvation temperature: 20 °C, cone gas flow: 10 L/h, desolvation gas flow: 800 L/h, 1 spectrum/s. Expected masses of oligonucleotide products were calculated using the AAT Bioquest RNA Molecular Weight Calculator. Deconvoluted mass spectra were obtained using the MaxEnt software (Waters Corporation).

i. Cryo-EM complex preparation

Briefly, the 70S complexes were formed by incubating 100 nM 70S ribosomes (prepared as described in Watson *et al.* 2020), 5 μ M mRNA encoding Met in the P site and UAG in the A site (IDT) (Table S5), 1 μ M each of fMet-NH-tRNA^{fMet} and β^2 -OH-BocK-NH-tRNA^{Pyl} (Table S5), and 100 μ M paromomycin (Sigma) in Grid Freezing Buffer (20 mM HEPES-KOH pH 7.5, 50 mM NH₄Cl, 50 mM KCl, 15 MgCl₂, 2 mM DTT) for 30 min at 37 °C.² Since the tRNAs were loaded non-enzymatically, paromomycin was added to stabilize the A-site tRNA and improve its cryo-EM density.⁷ The complexes were kept on ice prior to plunge freezing grids.

j. Cryo-EM sample preparation

The samples were prepared for imaging on 300 mesh R1.2/1.3 UltraAuFoil grids (Quantifoil) with an additional layer of float-transferred amorphous carbon support film. The grids were washed in chloroform prior to carbon floating. Before applying the sample, grids were glow discharged in a PELCO easiGlow at 0.37 mBar and 20 mAmp for 12 seconds. 4 μ L of sample was deposited onto each grid and incubated for 1 minute. Grids were blotted and plunge-frozen in liquid ethane with an FEI Mark IV Vitrobot using the following settings: 4 °C, 100% humidity, blot force 3, and blot time 2. Grids were clipped for autoloading and stored in liquid nitrogen.

k. Cryo-EM data collection

Cryo-EM data collection parameters are summarized in Supplementary Tables S1. Dose fractionated movies were collected on a Titan Krios G3i microscope at an accelerating voltage of 300 kV and with a BIO Quantum energy filter. Movies were recorded on a GATAN K3 direct electron detector operated in CDS mode. A total dose of 40 e⁻/Å² was split over 40 frames per movie. The physical pixel size was set to 0.81 Å and the super-resolution pixel size to 0.405 Å. Data collection was automated with SerialEM, which was also used for astigmatism correction by CTF and coma-free alignment by CTF. The defocus ramp was set to range between -0.5 and -1.5 μm.

l. Image Processing

Data processing was performed using RELION 5.0-beta-3 and cryoSPARC v4.6.2. MotionCor2 was used to motion correct the raw movies (binned to the physical pixel size estimated to be 0.81 Å during initial steps).⁸⁻¹⁰ CtfFind4 was used to estimate CTF parameters, and micrographs with poorly fitting CTF estimates were omitted after visual inspection. Particles were picked using the Laplacian-of-Gaussian autopicking method in RELION. Particles were then extracted at one-fourth binning of the full box size, and subjected to three rounds of 2D refinement to select 70S particles. The selected particles were imported to cryoSPARC,¹¹ where 3D classification was performed using the “Heterogeneous Refinement” job using a 70S reference volume generated from the coordinates of PDB entry 1VY4¹² using EMAN2.¹³ Classes corresponding to clean 70S volumes were selected and subjected to 50S-focused refinement, and exported back to RELION. To separate classes with rotations of the 30S subunit relative to the 50S subunit, 3D classification with no alignment was performed.¹⁴ Following this, masked classification for particles containing A-site tRNA was performed (with no alignments) and particles containing strong density for A-site tRNA were selected and re-extracted at full size. The particles were refined using the 3D auto-refine job in RELION, and then subjected to CTF Refinement,¹⁵ Bayesian Polishing,⁸ another round of CTF Refinement, and finally 50S and 30S focused refinements to improve global resolution. The global resolutions of the final 50S focused refinement maps were 2.14 Å for (*S*)-β²-OH-BocK, 2.29 Å for (*R*)-β²-OH-BocK (Supplementary Figures S7-S8).

m. Pixel Size Calibration

The pixel size was calibrated in UCSF ChimeraX¹⁶ using the “Fit to Map” function and the high resolution maps against the coordinates from the X-ray crystal structure PDB 4YBB.¹⁷ The best cross-correlation value was obtained at pixel size 0.8246 Å for (*S*)- β^2 -OH-BocK, 0.8235 Å for (*R*)- β^2 -OH-BocK. Half-maps for the refined volumes were rescaled to the calibrated pixel size in ChimeraX and post-processing was performed with these half-maps in RELION to obtain the FSC curves and final resolution estimates.

n. Modeling

PDB entry 8EBB containing Met-NH-tRNA^{Met} in both the P site and the A site was used as the starting model. The current structures contained tRNA^{Pyl} in the A site, and these coordinates were obtained from PDB 8UPY.¹⁸ Restraints for the (*S*)- β^2 -OH-BocK and (*R*)- β^2 -OH-BocK enantiomers were generated using eLBOW.¹⁹ Real space refinement of the coordinates was performed in PHENIX²⁰ and further adjustments to the model were done manually in Coot,²¹ mainly in the vicinity of the PTC. Further additions to the model included Mg²⁺ and K⁺ ions and water molecules. The linkage between A- and P-site tRNAs and monomers is modeled as an amide linkage to reflect experimental conditions for structure determination. The map-vs.-model FSC was calculated in PHENIX.²⁰

o. In vitro translation of peptides containing β^2 -OH monomers

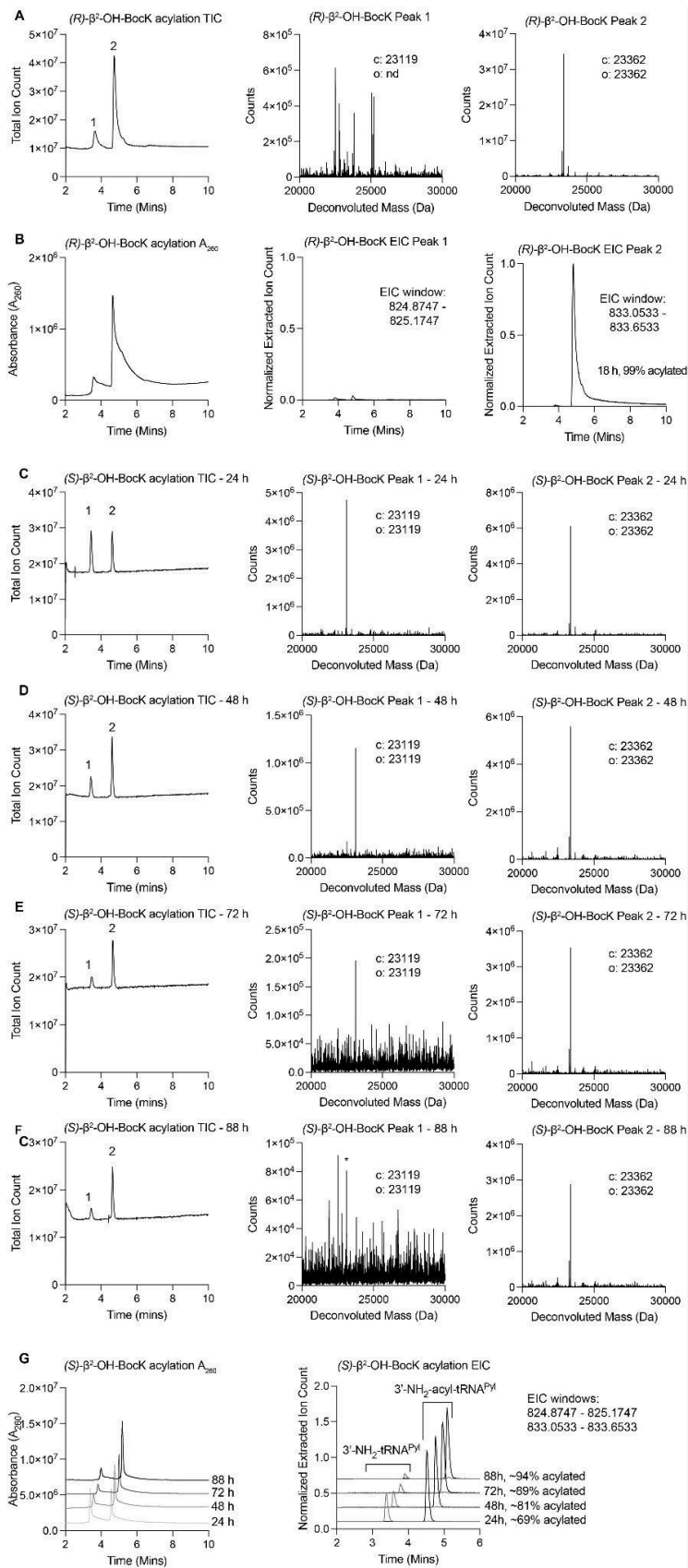
Peptide-1 (Table S6) was generated using *in vitro* transcription/translation (IVTT) from a template containing a T7 promoter, a ribosome binding site, the coding sequence for a short peptide with a FLAG-tag, and an amber stop codon. The stop codon was decoded by either 3'-tRNA^{Pyl}-BocK, 3'-tRNA^{Pyl}-(*R*)- β^2 -OH-BocK, or 3'-tRNA^{Pyl}-(*S*)- β^2 -OH-BocK, DNA templates were obtained as Ultramers (Table S4) from IDT and PCR amplified (5 ng of template, 0.5 μ M forward primer, 0.5 μ M reverse primer and Taq 2X Master Mix). Templates were purified using a DNA Clean and Concentrator Kit (Zymo Research). IVTT reactions were performed using a Δ RF Purexpress kit (NEB) where release factor 1 was omitted from the reactions. All Purexpress reagents (5 μ L Reagent A, 3.25 μ L Reagent B Δ RF123, 0.25 μ L RF2, and 0.25 μ L RF3) were added on ice, then 14-25 μ M acylated tRNA was added (adjusted for acylation efficiency as

determined by LCMS). Finally, the reaction was initiated by addition of 100 ng of DNA template. Reactions were incubated at 37 °C for 4 hours.

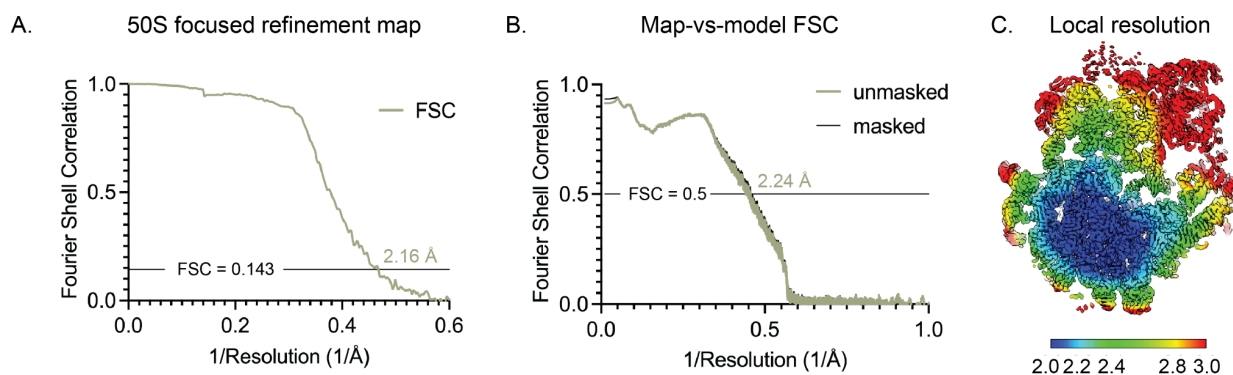
p. Purification and analysis of FLAG-tagged peptides

Anti-FLAG M2 Magnetic Beads (Millipore Sigma) were used to purify IVTT generated, FLAG-tagged peptides for downstream analysis. Anti-FLAG beads (12.5 µL) were washed with 100 µL wash buffer (50 mM Tris HCl pH 7.5, 150 mM NaCl) and the supernatant was removed from the beads. IVTT reactions were applied to the anti-FLAG beads and incubated at room temperature for 30 minutes. The supernatant was then removed, and the beads were washed 2X with 100 µL of wash buffer, and once with 100 µL of RNase free water. Elution buffer (12.5 µL) (100 mM glycine pH 2.8) was added to the beads and incubated at room temperature for 10 minutes. The supernatant was removed and analyzed by LCMS. Samples were resolved on an Agilent 1290 Infinity II HPLC using an Eclipse XDB C18 Column (1.8 µm, 2.1mm x 50 mm, 25 °C) (Agilent) with mobile phases A (water with 0.1 % [v/v] formic acid) and B (acetonitrile with 0.1 % [v/v] formic acid). The method began with a linear gradient from 0% B to 1% B for one minute, then a linear gradient was used from 1-91% B over five minutes at a flow rate of 0.5 mL/min, then subsequently washed with 91% B for 0.6 minutes, then a linear gradient decreased B from 91% to 1% for 1.1 minutes, finally the column was equilibrated 1% B for 1.3 minutes. The mass spectra of each sample was obtained on an Agilent 6530B QTOF AJS-ESI. The masses were analyzed using the MassHunter software (Agilent) by extracting the major ion corresponding to each peptide species (\pm 100 ppm) and integrating the subsequent extracted ion chromatogram.

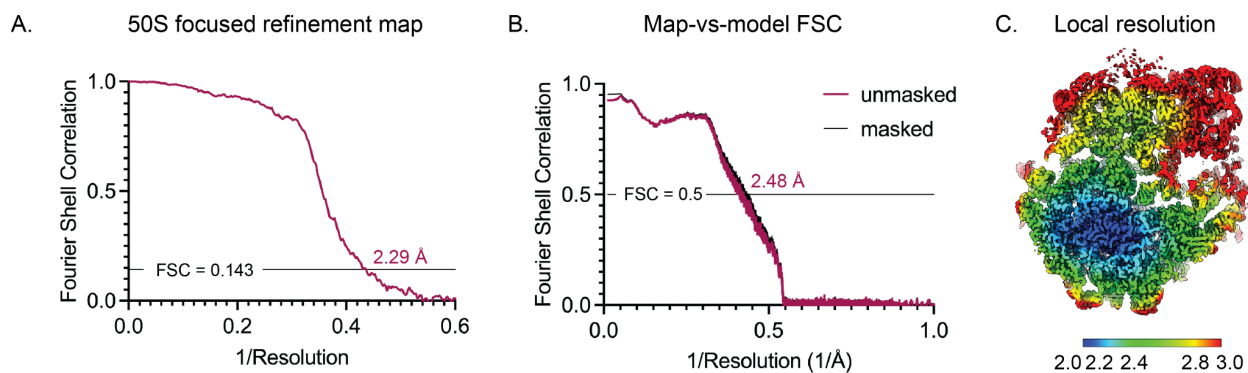
2. Supplementary Figures



Supplementary Figure S1: Acylation of 3'-NH₂-tRNA^{Pyl} with (*R*)-β²-OH-BocK and (*S*)-β²-OH-BocK. 3'-NH₂-tRNA^{Pyl} was acylated with (*R*)-β²-OH-BocK according to the protocol listed under **Materials and Methods subsection d** and subjected to LC-MS (**A-B**). The total ion chromatogram indicated the presence of two species one of low intensity and one of high intensity. Deconvolution of the high intensity peak yielded a major product of MW 23362 Da, corresponding to the MW of 3'-NH₂-tRNA^{Pyl} acylated with (*R*)-β²-OH-BocK. Deconvolution of the minor peak afforded a heterogeneous mixture of materials (**B**), none of which corresponded to the mass of unacylated 3'-NH₂-tRNA^{Pyl}. To further verify the absence of unacylated tRNA, we extracted ions between 823.8747 - 825.1747 Da and 833.0533 - 833.6533 Da, which correspond to the major m/z species of unacylated 3'-NH₂-tRNA^{Pyl} and (*R*)-β²-OH-BocK-acyl-3'-NH₂-tRNA^{Pyl}, respectively (**B**). Integrating these respective peaks to determine the percent of acyl-tRNA as a fraction of the total acylatable pool of tRNA indicated that over 99% of the acylatable tRNA was present as the monoacyl species. 3'-NH₂-tRNA^{Pyl} was acylated with (*S*)-β²-OH-BocK according to the protocol listed under **Materials and Methods subsection e** and subjected to LC-MS (**C-G**). Over a 4 day acylation protocol we consistently observed two peaks in the TICs, with the earlier peak attenuating over time. Deconvolution of the mass spectra of this peak yielded a product of 23119 Da, corresponding to the MW of unacylated 3'-NH₂-tRNA^{Pyl}. Deconvolution of mass spectra of the second peak yielded a product of 23362 Da, corresponding to the MW of 3'-NH₂-tRNA^{Pyl} acylated with (*S*)-β²-OH-BocK. Though unacylated 3'-NH₂-tRNA^{Pyl} was still detectable after 88 h, the deconvoluted mass spectra indicated that it was no longer the major mass under that peak (panel C, middle spectra, starred peak). Extraction of the ions between 823.8747 - 825.1747 Da and 833.0533 - 833.6533 Da indicated that over 94% of the acylated tRNA was present as the monoacyl (*S*)-β²-OH-BocK-acyl-3'-NH₂-tRNA^{Pyl}.

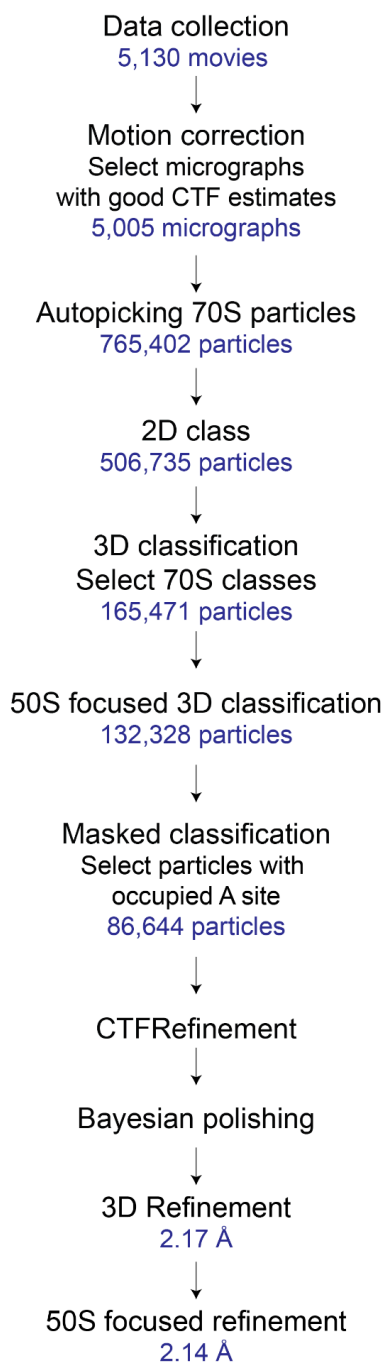


Supplementary Figure S2: Resolution of the 70S of the fMet-(*R*)- β^2 -OH-BocK complex. (A) FSC curve of the 50S subunit focused map (green) showing the global resolution of the map is 2.16 Å at the gold-standard cutoff value of 0.143. (B) Map-vs-model resolution is at 2.24 Å at FSC cutoff value of 0.5. (C) 50S focused map color coded by local resolution values.



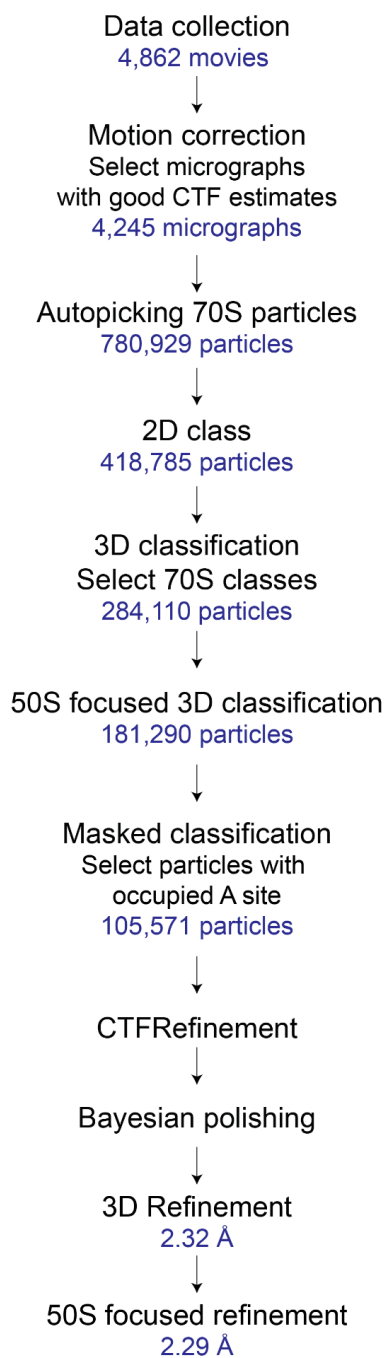
Supplementary Figure S3: Resolution of the 70S of the fMet-(*S*)- β^2 -OH-BocK complex. (A) FSC curve of the 50S subunit focused map (green) showing the global resolution of the map is 2.29 Å at the gold-standard cutoff value of 0.143. (B) Map-vs-model resolution is at 2.48 Å at FSC cutoff value of 0.5. (C) 50S focused map color coded by local resolution values.

Data processing steps for WT ribosome P-site fMet-NH-tRNA^{fMet} A-site (*R*)- β^2 -OH-Bock-NH-tRNA^{Pyl}

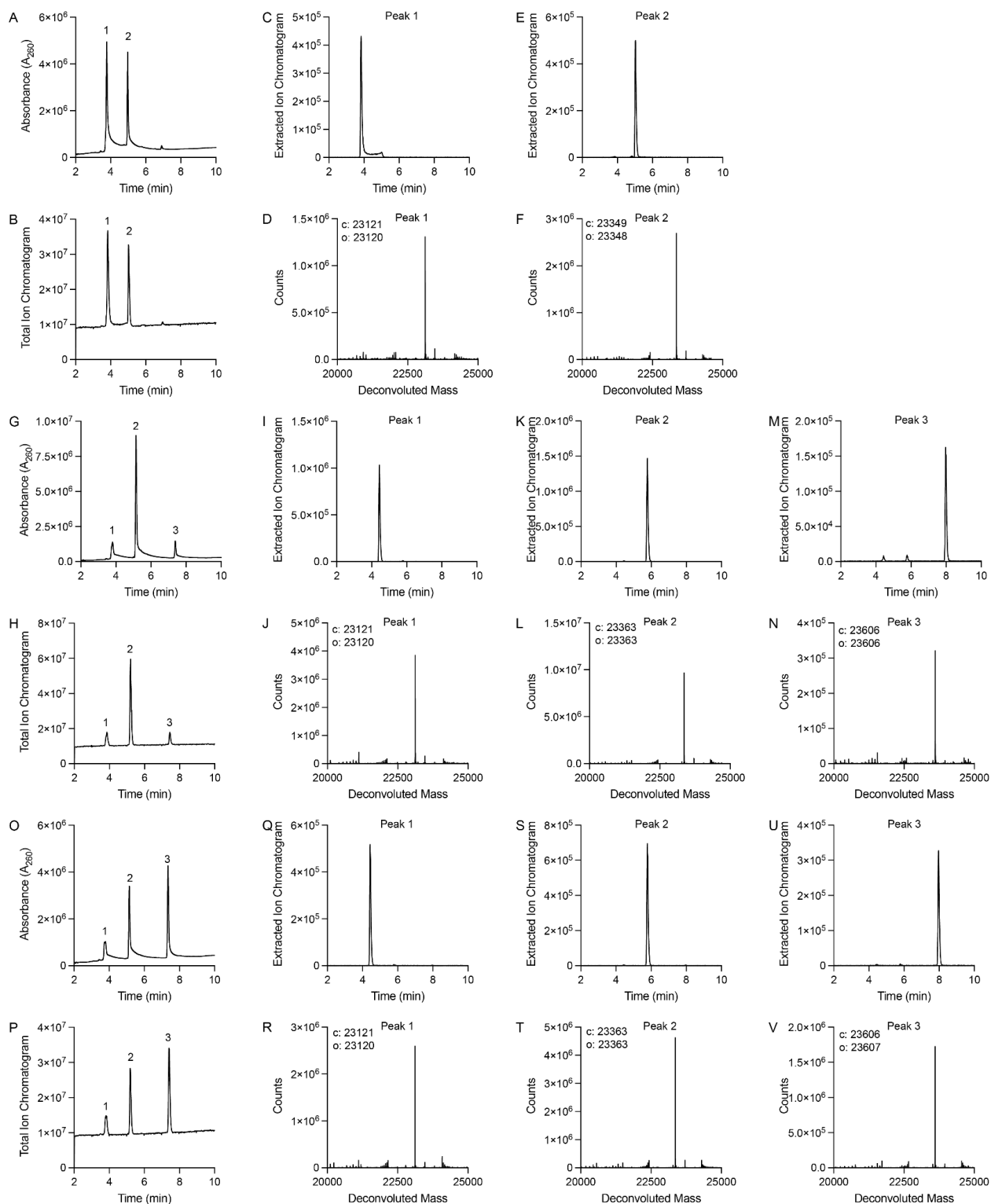


Supplementary Figure S4: Cryo-EM data processing workflow for the (*R*)- β^2 -OH-Bock containing complex. Number of movies, micrographs or particles, or resolution of the obtained volumes are indicated at each step.

Data processing steps for WT ribosome P-site fMet-NH-tRNA^{fMet} A-site (S)- β^2 -OH-BocK-NH-tRNA^{Pyl}

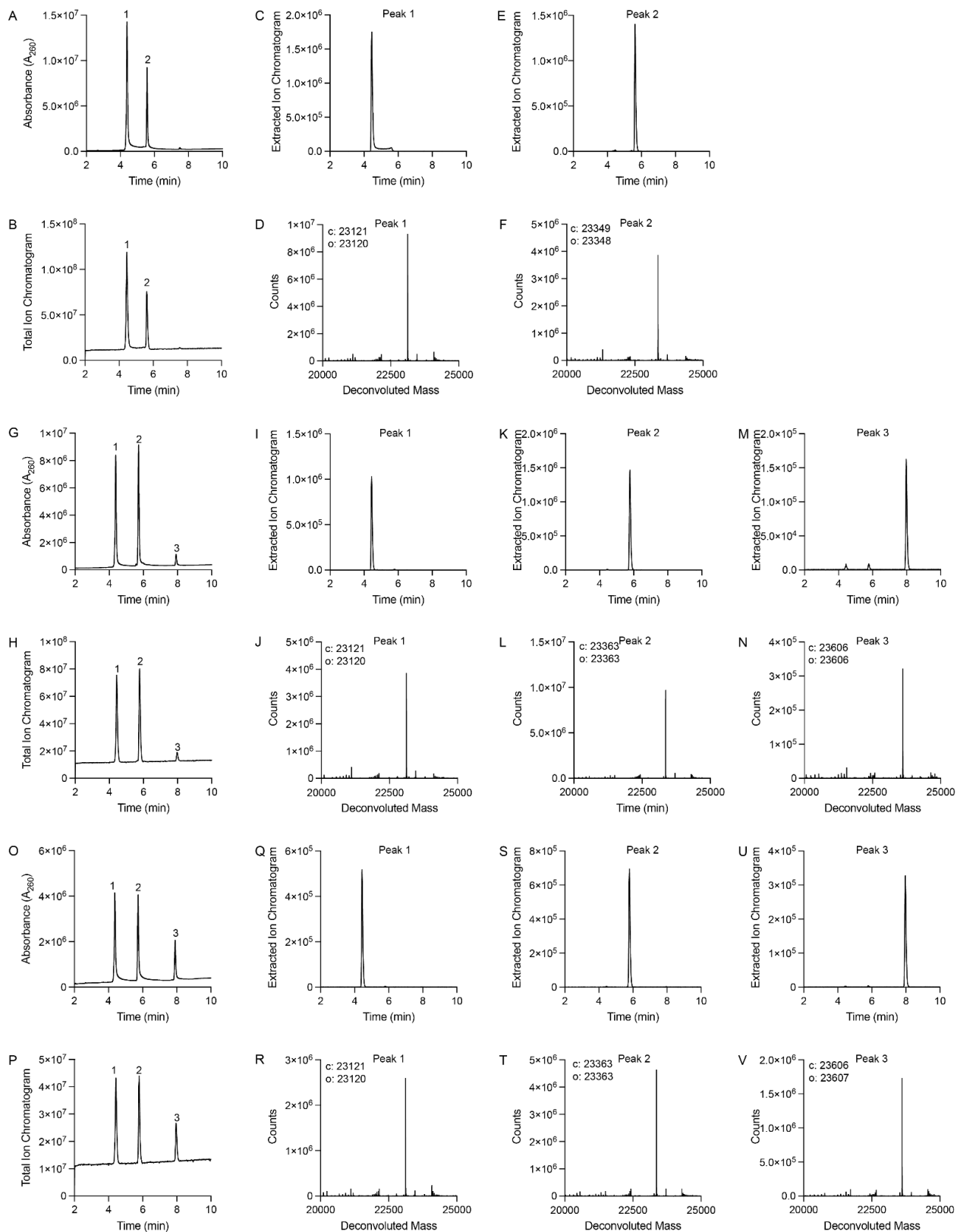


Supplementary Figure S5: Cryo-EM data processing workflow for the (S)- β^2 -OH-BocK containing complex. Number of movies, micrographs or particles, or resolution of the obtained volumes are indicated at each step.

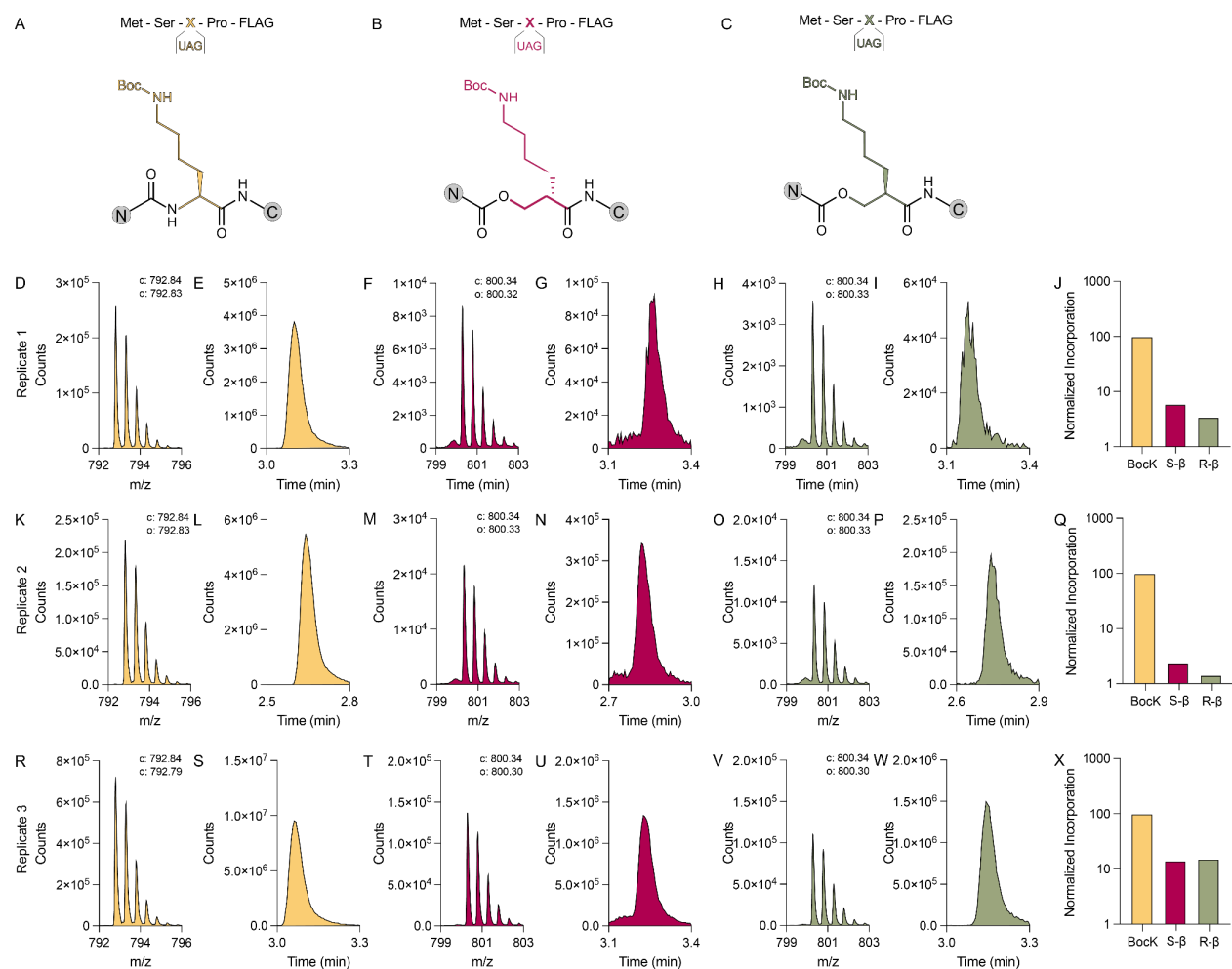


Supplementary Figure S6: Intact tRNA LC-MS of tRNA^{Pyl} acylated with three different monomers. The tRNA was acylated with each monomer using PylRS and LC-MS was used to determine the percentages of each species present which are tabulated in Table S3. These tRNA

were used in IVTT reaction Replicate 1 shown in Supplementary Figure S7. (A) Liquid chromatogram (LC) of acylation of tRNA^{PyI} with BocK. Peak 1 is tRNA^{PyI} and peak 2 is tRNA^{PyI}-BocK. (B) Total ion chromatogram (TIC) of acylation reaction in A. (C) Extracted ion chromatogram (EIC) of peak 1, starting material tRNA^{PyI}. (D) Mass spectra of peak 1 deconvoluted from m/z data. (E) EIC of peak 2, mono-acylated tRNA^{PyI}-BocK. (F) Mass spectra of peak 2 deconvoluted from m/z data. (G) LC of acylation of tRNA^{PyI} with (*S*)-β²-OH-BocK. Peak 1 is tRNA^{PyI}, peak 2 is (*S*)-β²-OH-BocK-tRNA^{PyI}, and peak 3 is ((*S*)-β²-OH-BocK)₂tRNA^{PyI}. (H) TIC of acylation reaction in G. (I) EIC of peak 1, starting material tRNA^{PyI}. (J) Mass spectra of peak 1 deconvoluted from m/z data. (K) EIC of peak 2, (*S*)-β²-OH-BocK-tRNA^{PyI}. (L) Mass spectra of peak 2 deconvoluted from m/z data. (M) EIC of peak 3, ((*S*)-β²-OH-BocK)₂tRNA^{PyI}. (N) Mass spectra of peak 3 deconvoluted from m/z data. (O) LC of acylation of tRNA^{PyI} with (*R*)-β²-OH-BocK. Peak 1 is tRNA^{PyI}, peak 2 is (*R*)-β²-OH-BocK-tRNA^{PyI}, and peak 3 is ((*R*)-β²-OH-BocK)₂-tRNA^{PyI}. (P) TIC of acylation reaction in O. (Q) EIC of peak 1, starting material tRNA^{PyI}. (R) Mass spectra of peak 1 deconvoluted from m/z data. (S) EIC of peak 2, (*R*)-β²-OH-BocK-tRNA^{PyI}. (T) Mass spectra of peak 2 deconvoluted from m/z data. (U) EIC of peak 3, di-acylated ((*R*)-β²-OH-BocK)₂-tRNA^{PyI}. (V) Mass spectra of peak 3 deconvoluted from m/z data. Calculated and observed masses are shown on each mass spectra.



Supplementary Figure S7: Intact tRNA LC-MS of tRNA^{Pyl} acylated with three different monomers. The tRNA was acylated with each monomer using PylRS and LC-MS was used to determine the percentages of each species present which are tabulated in Table S3. These tRNA were used in IVTT reaction Replicate 2 and 3 shown in Supplementary Figure S7. (A) Liquid chromatogram (LC) of acylation of tRNA^{Pyl} with BocK. Peak 1 is tRNA^{Pyl} and peak 2 is tRNA^{Pyl}-BocK. (B) Total ion chromatogram (TIC) of acylation reaction in A. (C) Extracted ion chromatogram (EIC) of peak 1, starting material tRNA^{Pyl}. (D) Mass spectra of peak 1 deconvoluted from m/z data. (E) EIC of peak 2, mono-acylated tRNA^{Pyl}-BocK. (F) Mass spectra of peak 2 deconvoluted from m/z data. (G) LC of acylation of tRNA^{Pyl} with SB2. Peak 1 is tRNA^{Pyl}, peak 2 is tRNA^{Pyl}-SB2, and peak 3 is tRNA^{Pyl}-SB2(x2). (H) TIC of acylation reaction in G. (I) EIC of peak 1, starting material tRNA^{Pyl}. (J) Mass spectra of peak 1 deconvoluted from m/z data. (K) EIC of peak 2, mono-acylated tRNA^{Pyl}-SB2. (L) Mass spectra of peak 2 deconvoluted from m/z data. (M) EIC of peak 3, di-acylated tRNA^{Pyl}-SB2(x2). (N) Mass spectra of peak 3 deconvoluted from m/z data. (O) LC of acylation of tRNA^{Pyl} with (*R*)-β²-OH-BocK. Peak 1 is tRNA^{Pyl}, peak 2 is tRNA^{Pyl}-(*R*)-β²-OH-BocK, and peak 3 is tRNA^{Pyl}-(*R*)-β²-OH-BocK(x2). (P) TIC of acylation reaction in O. (Q) EIC of peak 1, starting material tRNA^{Pyl}. (R) Mass spectra of peak 1 deconvoluted from m/z data. (S) EIC of peak 2, mono-acylated tRNA^{Pyl}-(*R*)-β²-OH-BocK. (T) Mass spectra of peak 2 deconvoluted from m/z data. (U) EIC of peak 3, di-acylated tRNA^{Pyl}-(*R*)-β²-OH-BocK (x2). (V) Mass spectra of peak 3 deconvoluted from m/z data. Calculated and observed masses are shown on each mass spectra.



Supplementary Figure S8: Incorporation of BockK, (S) - β^2 -OH-BockK, or (R) - β^2 -OH-BockK into peptides using *in vitro* transcription/translation. IVT reactions were analyzed using LC-MS to determine the mass of a peptide with sequence Met-Ser-X-Pro-Asp-Tyr-Lys-Asp-Asp-Asp-Lys, where X is BockK, (S) - β^2 -OH-BockK, or (R) - β^2 -OH-BockK. Extended and replicate data for Figure 4C-I. (A) Incorporation of BockK into a peptide over a recoded stop codon expanded below the sequence. The sequence of the peptide and corresponding chemical structure of the peptide highlighting the incorporated unnatural monomer (yellow) where (N) and (C) indicate the N- and C-termini of the peptide. (B) Incorporation of (S) - β^2 -OH-BockK into a peptide over a recoded stop codon expanded below the sequence. The sequence of the peptide and corresponding chemical structure of the peptide highlighting the incorporated unnatural monomer (red) where (N) and (C) indicate the N- and C-termini of the peptide. (C) Incorporation of (R) - β^2 -OH-BockK into a peptide over a recoded stop codon expanded below the sequence. The sequence of the peptide and corresponding

chemical structure of the peptide highlighting the incorporated unnatural monomer (green) where (N) and (C) indicate the N- and C-termini of the peptide. (D) Extracted ion chromatogram (EIC) of encoded peptide with BocK incorporation. (E) The m/z spectra of the peptide in D. (F) EIC of encoded peptide with (*S*)- β^2 -OH-BocK incorporation. (G) The m/z spectra of the peptide in F. (H) EIC of encoded peptide with (*R*)- β^2 -OH-BocK incorporation. (I) The m/z spectra of the peptide in H. (J) EIC integration values quantifying the relative yield of the peptides. Values have been normalized to BocK incorporation. (K-Q) and (R-X) are replicate data sets of D-J. For all peptides the calculated and observed masses are the $z = 2$ species.

3. Supplementary Tables

Table S1: Data collection and processing for WT *E. coli* ribosome complexes with β^2 -OH-BocK monomers.

Complex	(<i>R</i>)- β^2 -OH-BocK	(<i>S</i>)- β^2 -OH-BocK
Magnification	103,278	103,140
Voltage (kV)	300	300
Electron Exposure ($e^-/\text{\AA}^2$)	40	40
Defocus Range (μm)	-0.5/-1.5	-0.5/-1.5
Pixel Size (\AA)	0.8235	0.8246
Symmetry Imposed	C1	C1
Initial Particle Images	765,402	780,929
Final Particle Images	86,644	105,571
Map Resolution (\AA)	2.14	2.29
FSC Threshold	0.143	0.143

Table S2: Model Refinement Statistics for WT *E. coli* ribosome complexes with aminobenzoic acid monomers.

Model component	(<i>R</i>)- β^2 -OH-BocK	(<i>S</i>)- β^2 -OH-BocK
Model resolution (\AA)	2.3	2.5
FSC threshold	0.5	0.5
Map sharpening B factor (\AA^2)	-33.6298	-36.6824

Model composition		
Non-hydrogen atoms	145581	145518
Mg ²⁺ ions	320	320
Waters	3527	3473
Mean <i>B</i> Factors (Å ²)		
RNA	106.92	115.24
Protein	53.58	54.90
Waters	27.94	26.54
Other	77.78	74.41
R.m.s. deviations from ideal values		
Bond (Å)	0.006	0.003
Angle (°)	1.004	0.695
Molprobity score	2.05	2.32
Clash Score	4.56	9.84
Rotamer outliers (%)	5.01	4.29
Ramachandran plot		
Favored (%)	95.83	95.37
Allowed (%)	4.13	4.59
Outliers (%)	0.04	0.04
RNA validation		
Angles outliers (%)	0.016	0.0002
Sugar pucker outliers (%)	0.642	0.4207
Average suiteness	0.491	0.551

Table S3: Quantification of acylation from Supplementary Figures S6-S7 and corresponding IVTT replicates.

Monomer	Figure	IVTT	Unacylated	Monoacylated	Diacylated
BocK	S5A-F	Rep 1	56%	42%	2%
(<i>S</i>)-β ² -OH-BocK	S5G-N	Rep 1	5%	82%	13%

(<i>R</i>)-β ² -OH-BocK	S5O-V	Rep 1	2%	43%	54%
BocK	S6A-F	Rep 2-3	62%	37%	1%
(<i>S</i>)-β ² -OH-BocK	S6G-N	Rep 2-3	41%	53%	6%
(<i>R</i>)-β ² -OH-BocK	S6O-V	Rep 2-3	36%	44%	20%

Table S4: Sequences of DNA primers used in this study. mG represents 2'-O-methylguanosine modification

Primer name	Sequence
fMet_C1G_temp_Fw	5'-AATTCCTGCAGTAATACGACTCACTATAGGCGGGGTGGAGCAGCCTGGTAGCTCGTCGGGCTCATA-3'
fMet_C1G_temp_Rv(-A)	5'-GGTTGCGGGGGCCGGATTTGAACCGACGACCTTCGGGTTATGAGCCCGACGAGCTA-3'
fMet_C1G_amp_Fw	5'-AATTCCTGCAGTAATACGACTCAC-3'
fMet_C1G_amp_Rv(-A)	5'-GmGTTGCGGGGGCC-3'
Pyl_temp_Fw	5'-AATTCCTGCAGTAATACGACTCACTATAGGGGGACGGTCCGGCGACCAGCGGGTCTCTAA-3'
Pyl_temp_Rv(-A)	5'-GGCGAGAGACCGGGGCGTCGAACCCCGCTGGCTAGGTTTAGAGACCCGCTGGTC-3'
Pyl_amp_Fw	5'-AATTCCTGCAGTAATACGACTCA-3'
Pyl_amp_Rv (-A)	5'-GmGCGAGAGACCGGG-3'
IVTT Template	5'-GCCGAATTAATACGACTCACTATAGGGTAACTTTAACAAGGAGAAAACATGAGCTAGCCGGACTACAAAGACGATGACGACAAGTAAGTACTAGCATAACCCCTCTCTAAACGGAGGGTTTAGTCA-3'
IVTT Temp_Fw	5'-GCCGAATTAATACGACTCACTATAGGGTAACTTTAAC-3'
IVTT Temp_Rv	5'-TGACTAAACCCCTCCGTTTAGAGAGG-3'

Table S5: Sequences of RNA oligomers used in this study

RNA name	Sequence	Notes
tRNA ^{fMet}	5'-GGCGGGGUGGAGCAGCCUGGUAGCUCGUCG GGCU <u>CAUA</u> ACCCGAAGGUCGUCGGUCAAUC CGGCCCCCGCAACCA-3'	Anticodon underlined
tRNA ^{Pyl}	5'-GGGGGACGGUCCGGCGACCAGCGGGUCUCUA AAACCU <u>AGCC</u> AGCGGGGUUCGACGCCCCGGUC UCUCGCCA-3'	Anticodon underlined
mRNA	5'- GUAUA AGGAGG UAAAA <u>UGUAGU</u> AACUA-3'	Shine-Dalgarno sequence in bold, Met and UAG codons underlined

Table S6: Sequence of peptide synthesized during IVTT modification

Peptide name	Sequence
Peptide_1	Met-Ser-X-Pro-Asp-Tyr-Lys-Asp-Asp-Asp-Asp-Lys

4. References

- (1) Majumdar, C.; Walker, J. A.; Francis, M. B.; Schepartz, A.; Cate, J. H. D. Aminobenzoic Acid Derivatives Obstruct Induced Fit in the Catalytic Center of the Ribosome. *ACS Cent. Sci.* **2023**, *9* (6), 1160–1169. <https://doi.org/10.1021/acscentsci.3c00153>.
- (2) Watson, Z. L.; Ward, F. R.; Méheust, R.; Ad, O.; Schepartz, A.; Banfield, J. F.; Cate, J. H. Structure of the Bacterial Ribosome at 2 Å Resolution. *eLife* **2020**, *9*, e60482. <https://doi.org/10.7554/eLife.60482>.
- (3) Watson, Z.; Knudson, I.; Ward, F. R.; Miller, S. J.; Cate, J. H.; Schepartz, A.; Abramyan, A. M. TKTK Atomistic Simulations of the E. Coli Ribosome Provide Selection Criteria for Translationally Active Substrates. *bioRxiv* August 13, 2022, p 2022.08.13.503842. <https://doi.org/10.1101/2022.08.13.503842>.
- (4) Nissley, A. J.; Penev, P. I.; Watson, Z. L.; Banfield, J. F.; Cate, J. H. D. Rare Ribosomal RNA Sequences from Archaea Stabilize the Bacterial Ribosome. *Nucleic Acids Res.* **2023**, gkac1273. <https://doi.org/10.1093/nar/gkac1273>.
- (5) Walker, S. E.; Fredrick, K. Preparation and Evaluation of Acylated tRNAs. *Methods* **2008**, *44* (2), 81–86. <https://doi.org/10.1016/j.ymeth.2007.09.003>.
- (6) Fricke, R.; Swenson, C.; Roe, L. T.; Hamlish, N.; Ad, O.; Smaga, S.; Gee, C. L.; Schepartz, A. Orthogonal Synthetases for Polyketide Precursors. *bioRxiv* March 1, 2022, p 2022.02.28.482149.

- <https://doi.org/10.1101/2022.02.28.482149>.
- (7) Tsai, A.; Uemura, S.; Johansson, M.; Puglisi, E. V.; Marshall, R. A.; Aitken, C. E.; Korlach, J.; Ehrenberg, M.; Puglisi, J. D. The Impact of Aminoglycosides on the Dynamics of Translation Elongation. *Cell Rep.* **2013**, *3* (2), 497–508. <https://doi.org/10.1016/j.celrep.2013.01.027>.
 - (8) Zivanov, J.; Nakane, T.; Scheres, S. H. W. A Bayesian Approach to Beam-Induced Motion Correction in Cryo-EM Single-Particle Analysis. *IUCrJ* **2019**, *6* (1), 5–17. <https://doi.org/10.1107/S205225251801463X>.
 - (9) *New tools for automated cryo-EM single-particle analysis in RELION-4.0* | *Biochemical Journal* | Portland Press. <https://portlandpress.com/biochemj/article/478/24/4169/230248/New-tools-for-automated-cryo-EM-single-particle> (accessed 2023-01-22).
 - (10) *An image processing pipeline for electron cryo-tomography in RELION-5 - Burt - 2024 - FEBS Open Bio - Wiley Online Library*. <https://febs.onlinelibrary.wiley.com/doi/10.1002/2211-5463.13873> (accessed 2025-05-01).
 - (11) Punjani, A.; Rubinstein, J. L.; Fleet, D. J.; Brubaker, M. A. cryoSPARC: Algorithms for Rapid Unsupervised Cryo-EM Structure Determination. *Nat. Methods* **2017**, *14* (3), 290–296. <https://doi.org/10.1038/nmeth.4169>.
 - (12) Polikanov, Y. S.; Steitz, T. A.; Innis, C. A. A Proton Wire to Couple Aminoacyl-tRNA Accommodation and Peptide-Bond Formation on the Ribosome. *Nat. Struct. Mol. Biol.* **2014**, *21* (9), 787–793. <https://doi.org/10.1038/nsmb.2871>.
 - (13) Tang, G.; Peng, L.; Baldwin, P. R.; Mann, D. S.; Jiang, W.; Rees, I.; Ludtke, S. J. EMAN2: An Extensible Image Processing Suite for Electron Microscopy. *J. Struct. Biol.* **2007**, *157* (1), 38–46. <https://doi.org/10.1016/j.jsb.2006.05.009>.
 - (14) *The Structural Dynamics of Translation* | *Annual Review of Biochemistry*. https://www.annualreviews.org/doi/10.1146/annurev-biochem-071921-122857?url_ver=Z39.88-2003&rft_id=ori%3Arid%3Aacrossref.org&rft_dat=cr_pub++0pubmed (accessed 2023-01-24).
 - (15) (IUCr) *Estimation of high-order aberrations and anisotropic magnification from cryo-EM data sets in RELION-3.1*. <https://journals.iucr.org/m/issues/2020/02/00/fq5009/index.html> (accessed 2023-01-22).
 - (16) *UCSF ChimeraX: Structure visualization for researchers, educators, and developers - Pettersen - 2021 - Protein Science - Wiley Online Library*. <https://onlinelibrary.wiley.com/doi/10.1002/pro.3943> (accessed 2023-01-22).
 - (17) *High-resolution structure of the Escherichia coli ribosome* | *Nature Structural & Molecular Biology*. <https://www.nature.com/articles/nsmb.2994> (accessed 2023-01-22).
 - (18) Krahn, N.; Zhang, J.; Melnikov, S. V.; Tharp, J. M.; Villa, A.; Patel, A.; Howard, R. J.; Gabir, H.; Patel, T. R.; Stetefeld, J.; Puglisi, J.; Söll, D. tRNA Shape Is an Identity Element for an Archaeal Pyrrolysyl-tRNA Synthetase from the Human Gut. *Nucleic Acids Res.* **2024**, *52* (2), 513–524. <https://doi.org/10.1093/nar/gkad1188>.
 - (19) (IUCr) *electronic Ligand Builder and Optimization Workbench (eLBOW): a tool for ligand coordinate and restraint generation*. <https://journals.iucr.org/d/issues/2009/10/00/ea5105/index.html> (accessed 2025-05-02).
 - (20) Liebschner, D.; Afonine, P. V.; Baker, M. L.; Bunkóczi, G.; Chen, V. B.; Croll, T. I.; Hintze, B.; Hung, L.-W.; Jain, S.; McCoy, A. J.; Moriarty, N. W.; Oeffner, R. D.; Poon, B. K.; Prisant, M. G.; Read, R. J.; Richardson, J. S.; Richardson, D. C.; Sammito, M. D.; Sobolev, O. V.; Stockwell, D. H.;

Terwilliger, T. C.; Urzhumtsev, A. G.; Videau, L. L.; Williams, C. J.; Adams, P. D. Macromolecular Structure Determination Using X-Rays, Neutrons and Electrons: Recent Developments in Phenix. *Acta Crystallogr. Sect. Struct. Biol.* **2019**, *75* (10), 861–877. <https://doi.org/10.1107/S2059798319011471>.

- (21) Casañal, A.; Lohkamp, B.; Emsley, P. Current Developments in Coot for Macromolecular Model Building of Electron Cryo-Microscopy and Crystallographic Data. *Protein Sci. Publ. Protein Soc.* **2020**, *29* (4), 1069–1078. <https://doi.org/10.1002/pro.3791>.